Nanotechnology based affordable and label-free electrochemical approach for early cancer diagnosis

Amit K. Yadav[1], Damini Verma[1], Abhishek Kumar[2], Anant Narayan Bhatt[2], Pratima R. Solanki[1]*

[1]Special Center for Nanoscience, Jawaharlal Nehru University, New Delhi-110067, India

[2]Institute of Nuclear Medicine and Allied Sciences, Defence Research and Development Organization, New Delhi, India

***Corresponding Author:** pratimarsolanki@gmail.com; partima@mail.jnu.ac.in

Tel: 011-26704740/26704699

ABSTRACT

Herein, we report the results of the studies relating to developing a simple, sensitive, cost-effective, and disposable electrochemical-based label-free immunosensor for real-time detection of a new cancer biomarker, sperm protein-17 (SP17), in complex serum samples. An indium tin oxide (ITO) coated glass substrate modified with self-assembled monolayers (SAMs) of 3-glycidoxypropyltrimethoxysilane (GPTMS) was functionalized *via* covalent immobilization of monoclonal anti-SP17 antibodies using EDC(1-(3-(dimethylamine)-propyl)-3-ethylcarbodiimide hydrochloride) - NHS (N-hydroxy succinimide) chemistry. The developed immunosensor platform (BSA/anti-SP17/GPTMS@SAMs/ITO) was characterized *via* scanning electron microscopy (SEM), atomic force microscopy (AFM), contact angle (CA), Fourier transform infrared (FT-IR) spectroscopic, and electrochemical techniques such as cyclic voltammetry (CV), differential pulse voltammetry (DPV), and electrochemical impedance spectroscopy (EIS) techniques. The fabricated BSA/anti-SP17/GPTMS@SAMs/ITO immunoelectrode platform was used to measure changes in the magnitude of the current of the electrodes through an electrochemical CV and DPV technique. A calibration curve between current and SP17 concentrations exhibited a broad linear detection range of (100-6000 & 50-5500 pg mL^{-1}), with enhanced sensitivity (0.047 & 0.024 μA pg mL^{-1} cm^{-2}), limit of detection (LOD) and limit of quantification (LOQ) of 47.57 & 142.9 pg mL^{-1} and 158.58 & 476.3 pg mL^{-1}, by CV and DPV technique, respectively with a rapid response time of 15 min. It possessed exceptional repeatability, outstanding reproducibility, five-time reusability, and high stability. The biosensor's performance was evaluated in human serum samples, giving satisfactory findings obtained *via* the commercially available enzyme-linked immunosorbent assay (ELISA) technique, proving the

clinical applicability for early diagnosis of cancer patients. Moreover, various *in vitro* studies in murine fibroblast cell line L929 have been performed to assess the cytotoxicity of GPTMS. The results demonstrated that GPTMS has excellent biocompatibility and can be used for biosensor fabrication.

Keywords: 3-Glycidoxypropyltrimethoxysilane; Self-assembled monolayers; Indium tin oxide; Sperm protein 17; Cancer biomarker; Differential pulse voltammetry

INTRODUCTION

Cancer has recently become one of the leading causes of death worldwide. According to the World Health Organization (WHO) 2018 report, cancer kills almost 10 million people worldwide [1]. The world's population is expected to reach 8.3 billion by 2025, with more than 20 million new cases of cancer recorded each year [2][3]. Current research focuses on detecting cancer biomarkers in human fluids to aid in the early detection of cancer [4][5][6]. In this regard, the predictive importance of the Sperm protein 17 (SP17) in cancer patients has piqued researchers' curiosity. SP17 is a highly conserved mammalian protein found in the testis as well as spermatozoa which belongs to the cancer testis antigen (CTA) family and has been recognized as a tumor-linked antigen in several cancers occurring in humans, such as non-small cell lung cancer immunotherapy, neck, and head squamous cell carcinoma (HNSCC), multiple myeloma, and ovarian cancer. SP17 is composed of 151 amino acids (the full-length amino acid sequence has been shown in Fig. S7) and has an apparent 24.5 kDa molecular mass. Though the function of SP17s is not clear; however, it is assumed to play a role in egg zona pellucida interactions during the process of fertilization regulating sperm acrosomal response, capacitation, and maturation, but display high expression in cancer [7]. Thus, SP17 has been proposed as a potential biomarker for several cancers when its cancer-specific expression is combined. Traditional methods for cancer detection, such as biopsy, laparoscopy, hepatic angiography, CT-scan, ultrasonography, and enzyme-linked Immunosorbent Assay (ELISA), might take several hours/days from the time of testing and take days for result findings [8][9][10]. These procedures are unpleasant and long as well as sometimes necessitate expensive equipment and special care. This led to problems in the diagnosis of cancer in patients suffering from it and admitted to an emergency division. Therefore, a more sensitive, selective, user-friendly, and quick platform is urgently needed to meet the immediate diagnosis demands for detecting cancer markers at the initial disease stage. Sensors are important because they can provide real-time and accurate data in situations where current methods

may have gaps or limitations. This can be especially valuable in healthcare monitoring, where timely and precise information is essential for making informed decisions. Sensors can also help identify previously undetectable patterns and trends, leading to improved understanding and better problem-solving [11][12][13].

Electrochemical biosensors have gained appealing attention as an alternative to aid in quick diagnosis, giving improved intervention, and lowering the dissemination test time, which is very advantageous to reduce patient stress [14][15][16]. This is due to their high sensitivity, low cost, and portability. Further, a biosensing platform is critical for detecting target analytes with high sensitivity and specificity. Indium tin oxide (ITO) is an outstanding substrate in electrochemical and optical biosensors. In addition, compared to typical electrodes like glassy carbon electrodes, platinum, as well as gold, ITO is a cheap, stable, robust, and superb transparent conductive material. ITO-coated electrodes exhibit poor electro-catalytic activity, with a flat and low background current, which is advantageous to reduce noise in the case of an electrochemical biosensor [17]. Many studies have been conducted using ITO electrodes for their usage in electro-chemiluminescence, electrochemical nucleic acid biosensors, optical as well as electrical sensors analysis [18][19][20].

Various techniques have been used to modify ITO electrodes, including self-assembled monolayers (SAMs) creation [21], electro-polymerization [22], direct physical adsorption [23], electrophoretic deposition [24], and polymer thin film development [25]. Among them, SAMs are commonly used in biosensor production and play a vital role in developing electrochemical biosensors [26]. Self-assembling of silane molecules occurs with greater stability on the hydroxylated surface of ITO, allowing for efficient biomolecule coupling [27]. As a result, silanization-based SAMs formation may deliver a homogeneous layer on a specified surface for getting pre-determined surface attributes. Demirel et al. developed a DNA sensor utilizing a poly(N-isopropyl acrylamide) layer deposited on a silicon (Si) wafer [28]. 3-glycidoxypropyltrimethoxy silane (GPTMS) is an epoxy silane molecule used to create SAMs on oxide surfaces without needing a secondary cross-linker between the silane molecule and target antibodies. GPTMS is a bifunctional organ silane with three methoxy groups on one side and an epoxy ring on the other with the chemical formula $C_9H_{20}O_9Si$ [The 2D and 3D molecular structure of GPTMS has been given in Fig. S1(a and b)] [29][30]. In aqueous environments, epoxy groups are highly reactive to nucleophiles like acids, thiols, and amines and are relatively stable at neutral

pH [29]. Yang and co-workers fabricated a SAM-based epoxysilane biosensing platform for *Escherichia coli* (*E. coli*) O157: H7 detection based on the immobilization of affinity-purified antibodies [31].

In this study, we invented an amperometric immunosensor created on disposable ITO thin films utilizing biocompatible SAMs of GPTMS to detect a novel SP17 cancer biomarker for the first time. The GPTMS was self-assembled on the cleaned and activated surface of a hydroxyl-functionalized ITO electrode, forming an epoxy-functionalized highly structured SAMs layer at room temperature (RT). Subsequently, the anti-SP17 antibodies were covalently attached to this 3-glycidoxypropyltrimethoxy silane@ self-assembled monolayers (GPTMS@SAMs) layer without a cross-linker, providing a bio-recognition layer for SP17 biomarker detection. Cyclic voltammetry (CV), differential pulse voltammetry (DPV) and electrochemical impedance spectroscopy (EIS) techniques are vital for monitoring interface information between the electrode and the electrolyte solution and are thus used for electrochemical characterization. The immunosensor had good sensitivity and specificity in detecting the SP17 biomarker and was effectively utilized to measure SP17 concentrations in human serum samples, indicating the method's effectiveness. The results were then validated through the standard gold method, i.e., ELISA, for analysis of protein molecules. This immunosensor offers numerous advantages, including a simple production procedure, a low limit of detection (LOD), and minimal interference from other components found in real samples (human serum). Furthermore, the fabricated immunosensor was reusable five times, lowering the cost of the biosensor. The biocompatibility of nanomaterials is a critical consideration in the development of biosensors for biomedical applications. Thus, to the best of our knowledge, for the first time, the GPTMS was examined for its cytotoxicity in human lymphocyte cells using hemolysis and biocompatibility utilizing various *in vitro* studies in murine fibroblast cell line L929.

OBJECTIVES

1) Development of self-assembled monolayers (SAMs) of GPTMS onto ITO and their characterization

2) To study the biocompatibility of GPTMS through various *in-vitro* studies in L929 murine fibroblast cells

3) Fabrication of disposable nano-biosensing platform based on SAMs of GPTMS towards early detection of SP17 cancer biomarker

4) Validation of developed nano-biosensing platform in undiluted cancer patient serum samples

MATERIALS AND METHODS

Reagents and Instruments

Chemicals:

N-hydroxysuccinimide (NHS, $C_4H_5NO_3$, ≥98%); 3-glycidoxypropyltrimethoxysilane (GPTMS: molecular weight- 236.34; density- 1.07 g mL^{-1} at 25°C; Chemical formula- CO[Si](CCCOCC1CO1)(OC)OC; bp-120°C/2 mmHg); N-ethyl-N′-(3-dimethyl aminopropyl) carbodiimide hydrochloride (EDC, $C_8H_{17}N_3$, ≥97.0%); and bovine serum albumin (BSA, ≥ 96%) were brought from Sigma-Aldrich, India. Potassium hexacyanoferrate trihydrate [($K_4[Fe(CN)_6]$], ≥99.95%]; potassium ferricyanide(III) [($K_3[Fe(CN)_6]$], 99%]; acetone (CH_3COCH_3, 100); hydrogen peroxide (H_2O_2, 200); ethanol (CH_3CH_2OH, 99.9%); and sodium hydroxide pellets (NaOH, ≥97.0 %) were purchased from Fisher Scientific. Sodium chloride (NaCl, 99.9%); uric acid ($C_5H_4N_4O_3$, 99%); urea (NH_2CONH_2, 99.5%); oxalic acid ($(COOH)_2.2H_2O$, 99.5%); ascorbic acid ($C_6H_8O_6$, 99.7%); disodium hydrogen phosphate dihydrate (Na_2HPO_4, ≥99.5%) and sodium dihydrogen phosphate dihydrate (NaH_2PO_4, 99.5%) were procured from SRL. Antibodies of SP17 (anti-SP17), tumor necrosis factor-alpha (TNF-α), interleukin-8 (IL-8), cytokeratin 19 fragment (CYFRA-21-1), and SP17 were brought from My BioSource, USA. Various SP17 antigens, and an anti-SP17 antibody, were prepared in 20 mM Tris, 150 mM NaCl buffer (pH 8.0), and PBS having pH 7.4, respectively. ELISA KIT (Catalog No.- CSB-EL022451HU) of human sperm surface protein SP17 (SPA 17) was brought from CUSABIO. NaH_2PO_4 and $NaHPO_4$ were mixed well in Millipore water (Milli-Q) to prepare 0.2 M PBS, i.e., electrolyte solution with pH = 7.0, and kept in the refrigerator for further use. The ITO-coated glass substrate was purchased from Blazers, UK. Every chemical was utilized without any treatment and of analytical grade. Milli-Q (18.2 MΩ/cm) was employed for the whole experiment. Murine Fibroblast cells (L929) were retrieved from National Centre for Cell Sciences, Pune, India. The cells were propagated in High glucose Dulbecco's Modified Essential Medium (Sigma, USA), followed by 10% Fetal bovine Serum (Gibco, USA), and incubated at 37°C with 5% CO_2.

Instruments: The elemental mapping, composition, and surface morphologies of GPTMS@SAMs/ITO, as well as BSA/anti-SP17/GPTMS@SAMs/ITO electrode surfaces, were characterized using energy-dispersive X-ray (EDX) spectroscopy and scanning electron microscopy (SEM, JSM-IT 200, JEOL), functioned at an acceleration voltage of 5 k, respectively.

In addition, atomic force microscopy (AFM) with commercial silicon (Si) tip having a tip radius of <10 nm of the WITEC system in the tapping mode (applied in the standard cantilevers) was utilized for analyzing the surface modification steps of electrode fabrications. The images were taken at a scan rate of 5 μm s^{-1}, having a resolution of 256 × 256. To monitor surface end groups in different fabricated electrodes, Fourier transform infrared spectroscopy (FT-IR, Perkin Elmer, ATR Model, USA) for analyzing the chemical bonds from 4000 to 400 cm^{-1} wavenumber range was utilized. The dispersive Raman measurements were performed using EnSpectr R532, USA (laser of WITEC system having confocal microscope with 3 objectives) and excitation laser (780 nm) ranging from 500-2000 cm^{-1}. Moreover, for studying the water contact angle, the drop shape analyzer [KRUSS, Germany] was utilized to detect the hydrophobic/hydrophilic nature of fabricated electrodes. The SP17 concentrations in cancer patients' serum samples were estimated employing the ELISA plate reader of Biotek 800 TS microplate reader.

***In vitro* biocompatibility studies of GPTMS**

The biocompatibility of GPTMS-based nanomaterials was estimated using a case-by-case procedure in accordance with the International Standards ISO 10993-5 Third Edition 2009-06-01 "Biological Evaluation of Medical Devices – Part 5: Tests for *In vitro* Cytotoxicity. For determining the viability of GPTMS as a biocompatible nanomaterial for biosensor development, the cytotoxicity and biocompatibility of GPTMS were examined using an *in vitro* cell proliferation study as well as its interactions between the human cells at various time points by employing an inverted optical microscope.

Cellular Viability and Cytotoxicity: The percent cellular proliferation of the cells treated with various concentrations of GPTMS (5 μg to 2.5 mg mL^{-1}) w/v in culture medium was determined using 3-(4,5-dimethylthiazol-2-yl)-2,5-diphenyl tetrazolium bromide (MTT) assay as described earlier with slight modifications [32]. The cells were seeded in 96 well culture plates (5 $\times 10^3$ cells per well, 200 μL) as well as incubated overnight, followed by the addition of GPTMS. The cells were allowed to propagate for 48 h, and a further 20 μL of MTT (5 mg mL^{-1}) was added with 2 h incubation in the dark. The wells were then aspirated, and formazan crystals were dissolved by adding dimethyl sulfoxide (DMSO) (200 μL/well), followed by spectrophotometric determination at 540/630 nm.

The morphology and viability assessment in the adhesive form of the fibroblast cells was determined with the implementation of Calcein-acetoxymethyl (Calcein-AM) / Propidium Iodide

(PI) (Live/Dead) fluorescent staining [33]. The cells were plated in 24 well culture plates (25×10^3 cells per well, 500 µL) as well as subjected to various concentrations of GPTMS (5 µg - 50 µg) for 24 h. After incubation, the media was aspirated and incubated with Calcein-AM & PI (3 µM each), followed by fluorescence image acquisition using (Olympus CH30, Japan).

Clonogenicity and Migration Potential: The reproductive potential of the fibroblast cells incubated with various concentrations of GPTMS was determined using a Macro colony assay as described earlier [34]. The cells were first seeded in 60 mm cell culture Petri Dishes (PDs) (0.5×10^6 cells/PD), and PDs were treated with GPTMS (5 µg - 2.5 mg mL^{-1}) for 24h. The cells of each treatment group were then trypsinated and seeded in fresh 60 mm PDs (200 cells/PD) and left undisturbed for 7-9 days until colonies formed (50-100 cells/colony). The number of colonies was enumerated in both treatment and control groups by implementing crystal violet staining.

The *in vitro* cellular scratch assay model was adapted to determine the migration potential of GPTMS-treated fibroblast cells. The cells were seeded in 24 well culture plates ($25x10^3$ cells/well) overnight in a carbon dioxide (CO_2) incubator. A sterile pipette tip generated a scratch in the middle of the cell monolayer to mimic a wound. A single wash with PBS was given to remove the cellular debris, and GPTMS (5 µg - 50 µg) was added to the wells. Images of the scratch area were captured at 0 h, 12 h, and 24 h by 4X objective and 10X eyepiece (Olympus CH30, Japan), and the total cells migrated to the wound area were counted in both the treatment and control groups [35].

Hemolysis Rate: The varying concentrations of GPTMS (10 µg - 1 mg mL^{-1}, 500 µL) samples diluted in phosphate buffer silane (PBS) were prepared in 1.5 mL microcentrifuge tubes, and 2 % red blood cells (RBC) cell suspension (500 µL) was then added to the tubes, followed by incubation at 37 ^oC on a water bath. The mixture was then centrifuged at 100 g for 2 min, and the supernatant was further transferred to a 96-well plate and read at 540 nm to determine the extent of hemolysis [35]. PBS was used as a negative control, while distilled water was taken as a positive control. Hemolysis rate was calculated as (Eq.1):

$$Hemolysis\ rate\ (\%) = \frac{(OD_{sample} - OD_{negative\ control})}{(OD_{positive\ control} - OD_{negative\ control})} \times 100 \ldots\ldots\ldots \text{Eq. (1)}$$

\

Fabrication of biocompatible GPTMS@SAMs-based immunosensor

As reported in the literature, the GPTMS@SAMs were made on a pre-cleaned ITO glass plate with slight modification [36]. Before the immunosensor fabrication, the surface of the ITO electrode was cleaned by ultrasonication in ethanol and Milli-Q for 5 min. After drying, the cleaned ITO electrodes were firstly treated with a mixed solution of water: hydrogen peroxide: ammonium hydroxide ($H_2O/H_2O_2/NH_4OH$) in a 5:1:1 ratio for 60 min at 80 ℃ to get a uniform layer of hydroxyl (-OH) groups on the surface of ITO, followed by rinsing with water and drying protocol [37][38]. Next, the 1 % (v/v) solution of GPTMS in toluene was drop casted over the hydroxylated ITO electrodes overnight at RT (25 ^oC) to form a monolayer of epoxy silane comprising several active tails of epoxy groups to react rapidly with amino protein groups. This stage was essential as the silanization agent was coupled with the ITO electrode's hydroxylated terminals forming a Si-O-Si bonds monolayer [39]. The ITO electrode shape was made rectangular, having an active surface area of 0.5 cm × 0.5 cm, i.e., 0.25 cm^2, which is modified with GPTMS. Thus, all the electrodes were made under similar conditions. The SAMs formed electrode (GPTMS@SAMs/ITO) was then washed with water and toluene for removing other epoxysilane molecules from the surface and dried in the air at RT.

Following that, a stock solution of antibodies (anti-SP17 having 50 μg mL^{-1}) in PBS of pH 7.0 solution was prepared. The carboxyl (–COOH) terminal of the Fragment crystallizable (Fc) region of the antibody biomolecule was then activated utilizing the coupling chemistry of heterobifunctional cross-linkers such as EDC-NHS. Then, a solution of anti-SP17, EDC having 0.4 M (a coupling agent) and NHS having 0.1 M (an activator), was prepared in a 2:1:1 ratio and stored at 4 ^oC for 45 min to activate the carbonyl group of antibody molecules. Furthermore, 30 μL of antibody solution (activated) was drop casted onto the platform of GPTMS@SAMs/ITO as well as incubated at 25 ^oC in a humified chamber for 6 h to form an amide bond ($-CONH_2$) between –COOH ends of anti-SP17 and epoxy ends of GPTMS@SAMs through the EDC-NHS mechanism as displayed in scheme S1. The fabricated platform (anti-SP17/GPTMS@SAMs/ITO) was then washed thrice with PBS Of pH 7.4 for removing any extra anti-SP17 molecules. Lastly, 20 μL of 2 mg mL^{-1} bovine serum albumin (BSA) was drop casted to block the non-specific active areas of the prepared immunoelectrode. The developed immunosensing platform (BSA/anti-SP17/GPTMS@SAMs/ITO) was rinsed with PBS and kept in 4 °C until used again. Scheme 1(b) depicts a schematic representation of the fabrication of SAMs of a biocompatible GPTMS-based

immunosensing platform for SP17 detection in serum samples. The whole immunosensor construction pathway, principle, and chemical interactions of the biosensor are schematically displayed in Scheme 1(c).

Collection of patient blood samples

The Jawaharlal Nehru University (JNU), New Delhi, and the All-India Institute of Medical Sciences (AIIMS), New Delhi, gave all the necessary ethical permissions for the collection of patient samples. All cancer patient samples were received by following the procedure of AIIMs. Patients filled out the consent form during the collection of the blood sample. Before processing, these serum samples were taken in a pre-sterilized vial and stored undisturbed in the refrigerator for 20 min to allow coagulation of blood. Serum was then shifted in 5 mL centrifuge tubes as well as centrifuged (3000 rpm) for 15 min at 4 °C. To avoid freeze-thaw cycles, extraction of serum from the supernatant was done as well as its aliquots were made and kept at -80 °C until needed. The schematic representation of serum collection from cancer patients has been displayed in scheme 1(a).

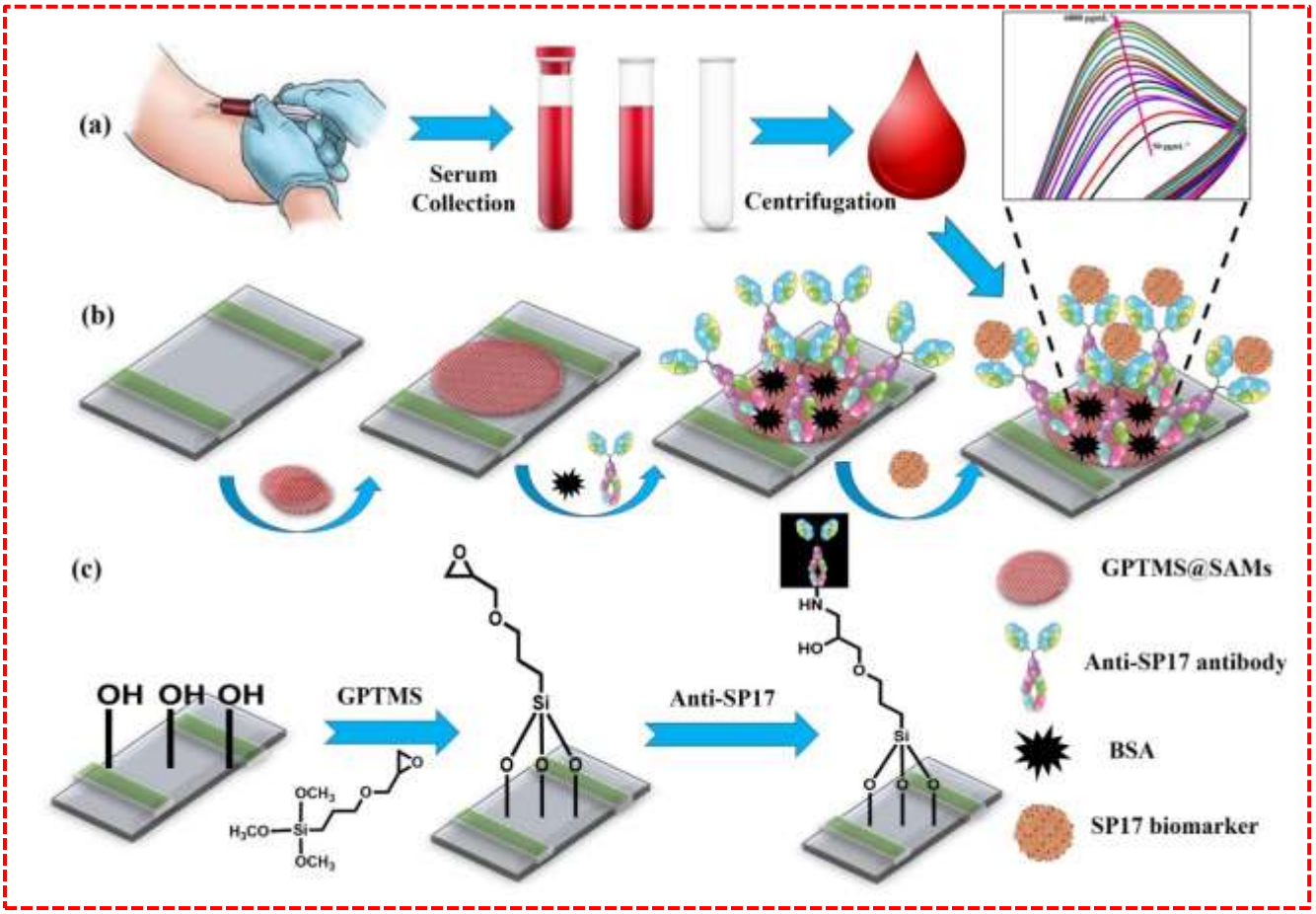

Scheme 1. A schematic representation for the formation and step-wise fabrication of an immunosensing platform for SP17 cancer biomarker detection in cancer patients' samples based on biocompatible and non-toxic SAMs of GPTMS.

Sample preparation of target analyte SP17

The stock solution of SP17 protein was prepared in 150 mM sodium chloride (NaCl) and 20 mM Tris buffer having pH 7.0, and its different concentrations were made from 100 pg mL^{-1} to 6000 pg mL^{-1} in PBS buffer (pH 7.4). The fabricated immunosensor was performed utilizing the DPV technique in PBS of pH 7.0 with 5 mM $[Fe(CN)_6]^{3-/4-}$. The practical utility of the developed immunosensor was done by validating the sensor in real samples such as blood.

Electrochemical measurements

The electrochemical response was investigated through cyclic voltammetry (CV), differential pulse voltammetry (DPV) as well as electrochemical impedance spectroscopy (EIS) techniques utilizing Autolab Potentiostat/ Galvanostat electrochemical analyzer (EcoChemie, The Netherlands). The CV measurements were performed at a 50 mVs^{-1} scan rate from -0.8 to +0.8 V potential. The EIS was measured at 0 voltage having a frequency ranging from 100 kHz to 10 Hz in the absence and presence of redox species i.e., $[Fe\ (CN)_6]^{3-/4-}$. The impedimetric signals were fitted to Randles equivalent circuit by using NOVA software. The studies were conducted to investigate the immobilization process and to monitor the interaction between anti-SP17 antibody and SP17 antigen in PBS (pH 7.0), which is made up of 0.9% NaCl, 0.2 M $Na_2HPO_4.2H_2O$, and 0.2 M $NaH_2PO_4.2H_2O$ in Milli-Q, with 5 mM $[Fe\ (CN)_6]^{3-/4-}$ as the redox species. For the electrochemical analysis, a three-electrode system involving silver/silver chloride (Ag/AgCl), platinum (Pt), and GPTMS-modified ITO glass acted as a reference, counter, and working electrodes, respectively. The complete electrochemical analysis was performed in triplicate (n = 3). Further, the oxygen scavenging has been done during the electrochemistry experiments by purging the solution with an inert gas, nitrogen before adding SP17 concentration. This removes the dissolved oxygen in the solution and replaces it with the inert gas, which does not interfere with the electrochemical reactions [40][41]. Moreover, the reference electrode (Ag/AgCl) also used to monitor and control the oxygen level in the solution, which measured the potential of the electrochemical cell. By monitoring the potential, any changes due to oxygen interference has been detected and corrected [41].

RESULTS AND DISCUSSION

Analytical Characterization

FTIR analysis

The Fig. 1A illustrates the FTIR curves of the anti-SP17 antibody immobilized ITO as well as GPTMS-modified ITO electrodes. FTIR spectra of each electrode were recorded in ATR mode in 4000-400 cm^{-1} wavenumber range at the resolution and scan of 4 cm^{-1} and 16, respectively. The findings depict the characteristic band of the epoxy group present in GPTMS at 847 cm^{-1} and 910 cm^{-1} [Fig. 1D] [42]. The bending and stretching vibrations were due to alkyl hydrogen at around 1563 cm^{-1} and 2941 cm^{-1}, respectively (Fig. 1C and 2B). The asymmetric stretching vibration of Si–O–Si gave a strong, broad band at 1080 cm^{-1}. The 814 and 910 cm^{-1} bands occur due to Si–O–Si symmetric and Si-OH asymmetric stretching vibrations, respectively. Also, the O–Si–O vibrations occurred at 448 and 533 cm^{-1}. A weak band appeared at 678 cm^{-1} due to the out-of-plane bending vibrations of the C–OH groups [36] (Fig. 1E). After the immobilization of the anti-SP17 antibody, the distinctive bands of -NH bending and C=O stretching were seen at 1077 cm^{-1} and 1644 cm^{-1}, respectively. The occurrence of the band at 1077 cm^{-1} corresponding to –CO stretching was reported, produced between the anti-SP17 –COOH group and GPTMS $–NH_2$ group, thus affirming the binding of anti-SP17 to the surface of silane-modified ITO electrode. These bands confirm the amide formation between the anti-SP17 antibody terminal amino groups and GPTMS epoxy groups. Additionally, Fig. 1A also depicts a broad band ranging from 3000 to 3400 cm^{-1}, which is due to the –OH and –NH bond stretching vibrations of water molecules. The amide groups in the protein backbone of antibodies, such as the primary amine group ($-NH_2$) and the carboxylic acid group (-COOH) of the amino acids, contribute to the characteristic peaks in the amide I (1650-1700 cm^{-1}) and amide II (1550-1630 cm^{-1}) regions of the FTIR spectra [43]. In addition, antibodies also contain hydroxyl (-OH) groups in the side chains of some amino acids, such as serine, threonine, and tyrosine. The hydroxyl groups contribute to the broad peak in the 3200-3600 cm^{-1} region of the FTIR spectra. On the other hand, GPTMS is a silane coupling agent containing no hydroxyl (-OH) groups, thus not showing the band at 3000 to 3400 cm^{-1} in the FTIR spectra.

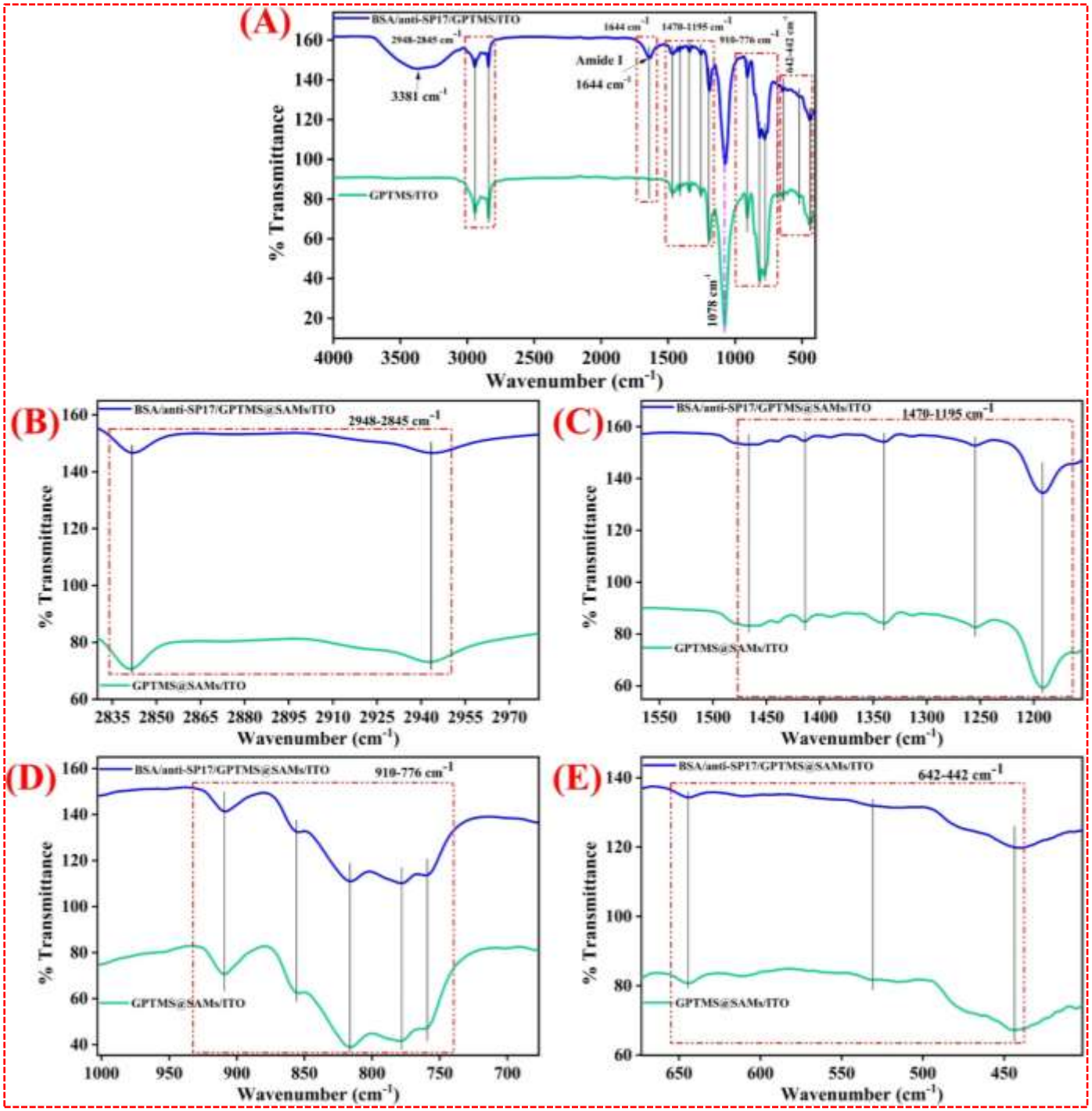

Figure 1: (A) FT-IR spectra of GPTMS@SAMs/ITO electrode and BSA/anti-SP17/ GPTMS@SAMs/ITO immunoelectrode; (B) details of 2948-2845 cm^{-1} band; (C) details of the 1470-1195 cm^{-1} band; (D) details of the 910-776 cm^{-1} band; and (E) details of the 642-439 cm^{-1} band.

Raman analysis

The chemical and molecular findings of the working surface electrode were estimated with the help of Raman spectroscopy. This technique helps in proving the practical data for the particular interactions taking place between different biomolecules and molecules. The relative shift of the Raman band and variation in intensity depicts the chemical communication between biomolecules and SAMs [44]. Therefore, SAMs formation and the immobilization of antibody on the surface of the ITO electrode was performed utilizing this technique. As shown in Fig. 2A(a), bands at 911 cm^{-1} and 852 cm^{-1} were attributed to the epoxy ring stretching of GPTMS. Considering calculated Raman activities, the intensive Raman bands observed at 3056 cm^{-1} and 3006 cm^{-1} are CH_2 and CH stretching modes connected to the epoxy ring. Three bands observed in Raman spectra at 2944 cm^{-1}, 2844 $cm^{-1,}$ and 2839 cm^{-1} are assigned to CH_3 stretching modes of the methoxy groups (Fig. 2E). In the frequency region 1500–1100 cm^{-1}, the fundamentals at 1480 cm^{-1} (υ22), 1389 cm^{-1} (υ35), 1196 cm^{-1} (υ 43) and 1162 cm^{-1} (υ 44) have been assigned as CH_2 group vibrations of propyl chain. A strong Raman band observed at 1256 cm^{-1} is characteristic of the epoxy group [45] (Fig. 2D). A strong IR band observed at 1159 cm^{-1} (υ45) is a pure vibration of methoxy groups that consists of CH_3 rocking combined with CO stretching. The weak Raman bands observed at 1136 cm^{-1} (υ49), 1114 cm^{-1} (υ53), and 1106 cm^{-1} (υ54) are the vibrations of the glycidoxy group. The band at 530 cm^{-1} is assigned as the scissoring vibrations of the CCO valence bond angle in the glycidoxy group (Fig. 2C). Bands observed at 480 cm^{-1} and 443 cm^{-1} are described as COC and SiO_3 symmetrical deformations, respectively. A moderate Raman band observed at 246 cm^{-1} is assigned as SiO_3 rocking, SiOC deformation, CCO, and CCC scissoring connected with SiO_3 asymmetric deformation (Fig. 2B)[46].

Furthermore, this technique is the most suitable for analyzing the amide bonds. The characteristic bands of amide III, II, and I bonds were observed between 1235 and 1350 cm^{-1}; 1480 and 1570 cm^{-1}, as well as 1650 and 1680 cm^{-1}, respectively, on GPTMS-modified ITO electrodes [47] (Fig. 2A(b)). After immobilizing the anti-SP17 antibody, amide III, I, and II bonds were found at 757, 905, and 757 cm^{-1}, respectively, confirming the binding of anti-SP17 on the GPTMS@SAMs/ITO electrode surface (Fig. 2D).

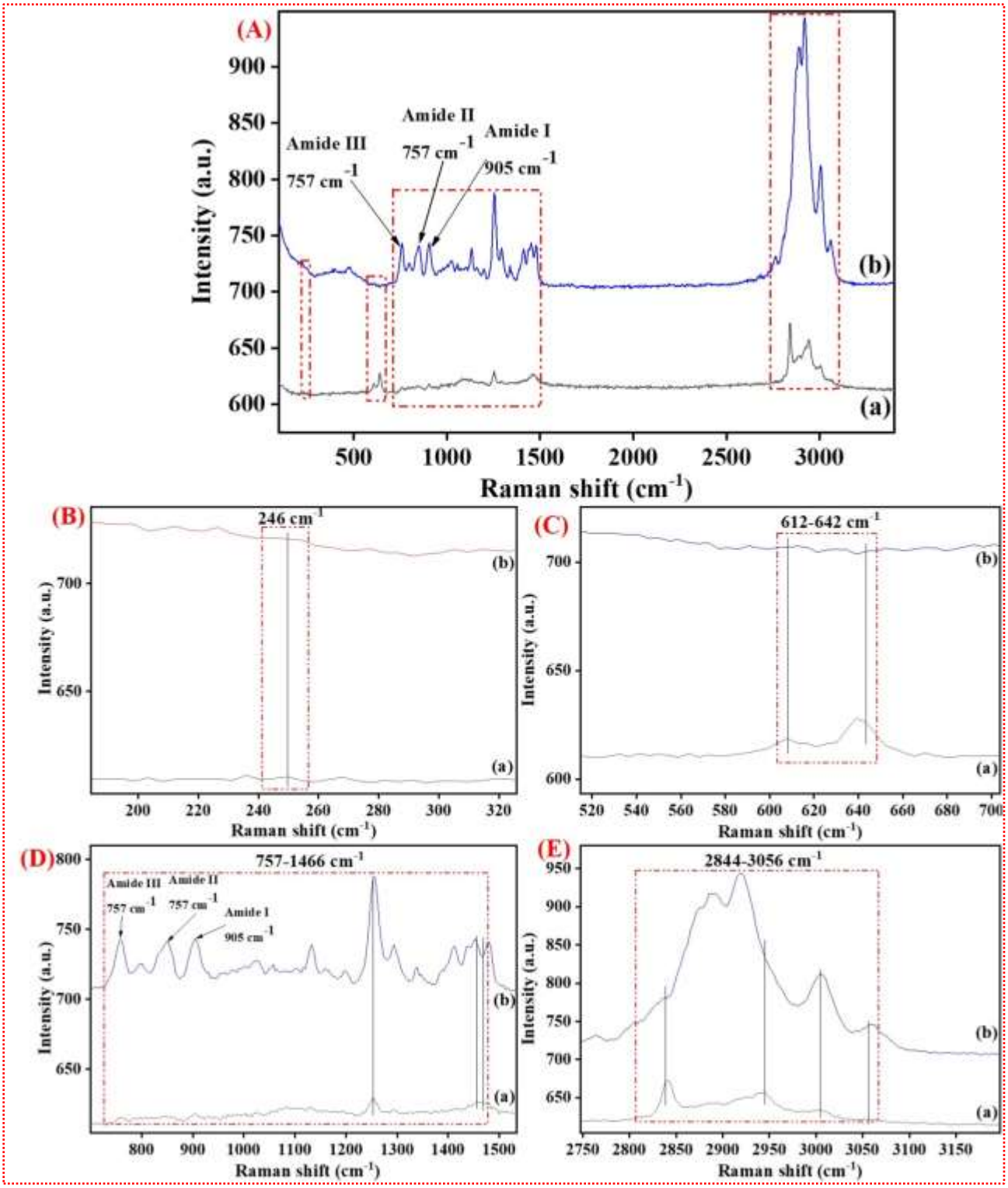

Figure 2: (A) Raman spectra of (a) GPTMS@SAMs/ITO electrode and (b) BSA/anti-SP17/ GPTMS@SAMs/ITO immunoelectrode; (B) details of the 246 cm^{-1} band; (C) details of the 612-642 cm^{-1} band; (D) details of the 757-1466 cm^{-1} band; and (E) details of the 2844-3056 cm^{-1} band.

Contact angle analysis

The technique of sessile drop was performed for contact angle (CA) studies for investigating the hydrophilicity or hydrophobicity nature of the SAMs of the GPTMS surface, as well as for every step-wise alteration [Fig. S2(a-d)]. The contact angles of these electrodes were evaluated using water droplets spread onto GPTMS@SAMs films as a qualitative method for assessing the relative variation of hydrophobic/hydrophilic behavior of the ITO, GPTMS@SAMs/ITO, anti-SP17/GPTMS@SAMs/ITO and BSA/anti-SP17/GPTMS@SAMs/ITO immunoelectrodes [48]. The value of CA for ITO was 99.7° as depicted in Fig. S2(a), which decreased to 86.5° [(Fig. S2(b)] showing the GPTMS monolayer fabrication on the hydrolyzed ITO (GPTMS@ SAMs/ITO). The reduced CA value could be ascribed to hydrophilic epoxy group presence in the GPTMS, which establishes a convenient platform for the immobilization of anti-SP17 antibodies. The value of CA was further reduced to 43.2° [Fig. S2(c)] and 25.6° [Fig. S2(d)] after immobilizing the biomolecules such as anti-SP17 antibodies as well as BSA, respectively. The reduction in CA value is due to the hydrophilic nature of electrodes (BSA/anti-SP17/GPTMS@SAMs/ITO and anti-SP17/GPTMS@SAMs/ITO) which proves the covalent attachment of anti-SP17 antibodies as well as BSA on the surface of GPTMS@SAMs/ITO electrode. This immunoelectrode hydrophilicity enhances the increased attachment of antigen (in PBS buffer), thus improving immunosensor sensitivity [7].

Morphological Characterization

Scanning electron microscopy *(*SEM) and atomic force microscopy (AFM) methods are recognized as powerful techniques for studying the surface morphology of various surfaces of electrodes. The images of SEM, as well as AFM of the GPTMS@SAMs/ITO and anti-SP17/GPTMS@SAMs/ITO immunoelectrode, are shown in Fig. 3(A and E) and Fig. 3(B-D and F-H), respectively, confirming the step-by-step alteration done on the sensing platform. It could be observed that GPTMS@SAMs/ITO and anti-SP17/GPTMS@SAMs/ITO immunoelectrode surfaces had evidently diverse morphologies. The image of SEM [Fig. 3(A)] and AFM [Fig. 3(B-D)] of the GPTMS@SAMs/ITO electrode shows a dense surface structure revealing SAMs formation. The GPTMS monolayer distribution on the surface of ITO is dense, thick, and uniform, with insufficient homogeneous agglomerates. The average roughness (Ra) value of the GPTMS@SAMs/ITO electrode was -484.4 nm on a 5×5 mm scale which confirmed the highly ordered and dense SAMs over the ITO surface. The formed SAMs 3D network layer was

appropriate for anti-SP17 antibody immobilization owing to the increased GPTMS layer surface area. The sole assembly of the GPTMS layer can deliver an advantageous microenvironment for the proteins for retaining its good bioactivity. Fig. 3(E) and Fig. 3(F-H) depict SEM as well as AFM images, respectively, for the anti-SP17 antibody-immobilized ITO electrode surface. It could be observed from the figure that the surface morphology of the electrode was modified in comparison to the GPTMS@SAMs/ITO electrode, followed by the uniform distribution of immobilized antibodies for binding to anti-SP17 antibodies homogenously. The antibodies' homogeneous immobilization offers a reproducible and sensitive response to the electrode. The bigger size and globular structure of anti-SP17 antibodies binded to the GPTMS@SAMs/ITO electrode surface are clearly visible. Therefore, an increase was seen in Ra (0.7 nm) on a 5×5 mm scale as compared to GPTMS@SAMs/ITO (Ra= -484.4). Biomolecules' covalent attachment to the GPTMS functional groups in a similar style shows more compactness of anti-SP17 molecules at the GPTMS@SAMs/ITO electrode.

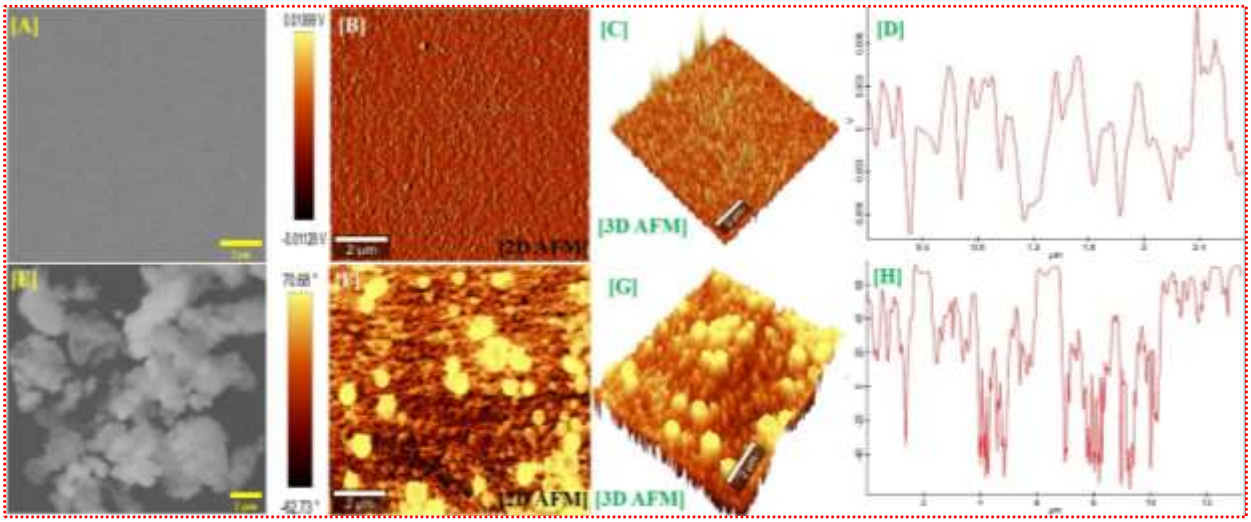

Figure 3: Scanning electron microscopy images of GPTMS@SAMs/ITO electrode (A) and anti-SP17/GPTMS@SAMs/ITO immunoelectrode (E); 2D AFM (B and F), 3D AFM (C and G), and cross-section line images of GPTMS@SAMs/ITO electrode and anti-SP17/GPTMS@SAMs/ITO immunoelectrode, respectively.

Moreover, Energy-dispersive X-ray spectroscopy *(*EDX) with elemental mapping studies was also conducted for defining the elemental compositions of ITO surface after modification of SAMs with GPTMs (GPTMS@SAMs/ITO) and anti-SP17 antibodies (anti-SP17/GPTMS @SAMs/ITO), as illustrated in Fig. S3(A) and Fig. S3(B), respectively. The analysis showed that the GPTMS@SAMs/ITO electrode had significant binding energies peaks of Indium (In), Silicon

(Si), Oxygen (O), and carbon (C) elements, suggesting the high purity of the SAMs formation. The Si element (orange) could be clearly visible in Fig. S3(E) that arises from molecules of GPTMS epoxysilane as well as its ratio was estimated as 6.77 %. This finding shows GPTMS coating on the surface of ITO. Next, after modification with anti-SP17 antibodies (anti-SP17/GPTMS@SAMs/ITO bioelectrode), it showed C, O, and Si elements [Fig. S3(B)]. Moreover, EDX spectra also represent the N atom, showing successful anti-SP17 antibodies biomolecule immobilization on the GPTMS@SAMs/ITO electrode surface. This peak for the N atom arises due to the amino acids chain of antibodies biomolecules. Thus, these images of EDX demonstrate the presence of anti-SP17 biomolecules on the GPTMS@SAMs/ITO electrode. In addition, the elemental mapping profile of GPTMS@SAMs/ITO [Fig. S3(C-F) and anti-SP17/GPTMS@SAMs/ITO [Fig. S3(G-J)] indicates the homogeneous distribution of C, O, Si, In, and N elements.

Biocompatibility studies

The biocompatibility of nanomaterials is a critical consideration in the development of biosensors for biomedical applications. The use of nanomaterials in biosensor fabrication has shown great promise in enhancing the sensitivity, selectivity, and stability of biosensors. However, it is essential to ensure that these nanomaterials are biocompatible to avoid any adverse effects on living organisms. Therefore, several studies have been conducted to evaluate the biocompatibility and cytotoxicity of GPTMS in human lymphocyte cells using hemolysis and several *in vitro* studies in murine fibroblast cell line L929 in the current work.

In-vitro compatibility and cytotoxicity of GPTMS

The cytotoxicity profiling of the GPTMS, including cellular viability, morphology determination, and live/dead cell assessment, was performed in a murine fibroblast cell line, L929. These cells are highly utilized in cytotoxicity determination studies as they closely resemble human dermal fibroblasts [49]. After incubation, the percent proliferation of cells with various concentrations of GPTMS (5 µg to 2.5 mg mL^{-1}) w/v in a culture medium was determined using MTT cellular viability assay. The obtained results showed that the cells treated with 5 µg to 50 µg GPTMS had no significant effect on the cellular viability, but relative cellular proliferation inhibition of up to 20 % (generally considered safe) was observed at conc. 100 µg to 250 µg [Fig. 4A(a)]. Further increasing the conc. of GPTMS from 250 µg to 2500 µg proved cytotoxic to fibroblast cells. The fibroblast cells were then observed for morphological changes induced by the treatment of

GPTMS. The morphology was studied by Calcein-AM (Live) and PI (Dead) stained cells observed by fluorescence imaging. The resulting photomicrographs of fibroblast cells treated with GPTMS (5 µg to 50 µg) showed morphology which was comparable with control (untreated) cells, and no significant induction in the dead cell population was observed. [Fig. 4A(c)]. These results indicate the relatively safe nature of GPTMS up to 50 µg mL^{-1} concentration.

Hemolysis analysis of GPTMS

A small tendency for inducing hemolysis is a vital necessity for the fabrication of biocompatible biosensors. The existence of hemolytic material with serum may destroy the red blood cells along with the liberation of free plasma hemoglobin in the supernatant of the test solution, which may affect the transportation of oxygen, inducing stress and toxic effects to other organs or the kidneys [50][51]. The GPTMS solution ranging from 10 µg to 1 mg mL^{-1} (in PBS) was subjected to hemolysis rate analysis in whole human blood for hemocompatibility assessment. The polymer compound was found to be non-hemolytic at all the tested concentrations and was comparable with negative control (PBS), while an apparent rupture of RBCs and release of hemoglobin could be seen in erythrocytes treated with the positive control (distilled water), as shown in Fig. 4A(b) The lower hemolysis rate of the formulation represents the better hemocompatibility of the polymer [52][35].

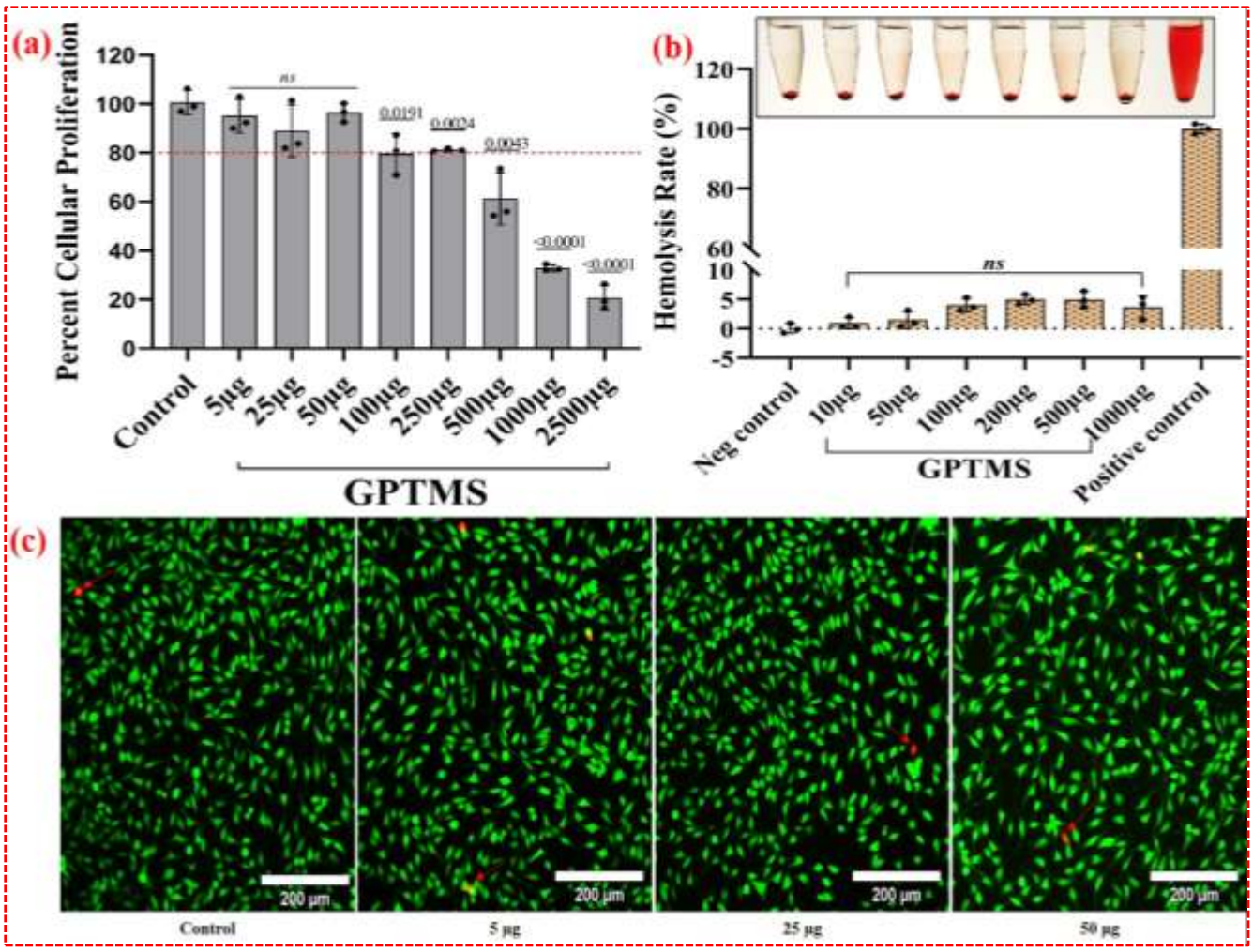

Figure 4A: (a) Cell viability of murine fibroblast L929 cell lines treated with GPTMS at different concentrations after 48 h. IC50 of GPTMS was found to be >500 µg mL^{-1}; (b) Hemolysis test of blood after centrifugation at different concentrations of GPTMS observed under UV absorbance at 540 nm; and (c) Morphology and viability assessment of L929 cell line in the adherent form Calcein-AM & PI fluorescent staining fluorescence imaging.

Reproductive and Migration potential of GPTMS

To further substantiate the *in-vitro* cytotoxicity findings, a clonogenic survival assay was performed to estimate the treatment-induced change in cell plating efficiency (PE). The results obtained showed no significant difference in the PE of 5 µg to 100 µg of GPTMS treated cells, but a slightly decreased PE could be observed in 250 µg mL^{-1} GPTMS (55% PE) treated cells as compared with untreated control cells (69 % PE) [Fig. 4B(a) and (b)]. It could be interpreted from these results that the fibroblast cells treated with GPTMS (up to 100 µg) are not losing any of their reproductive potentials.

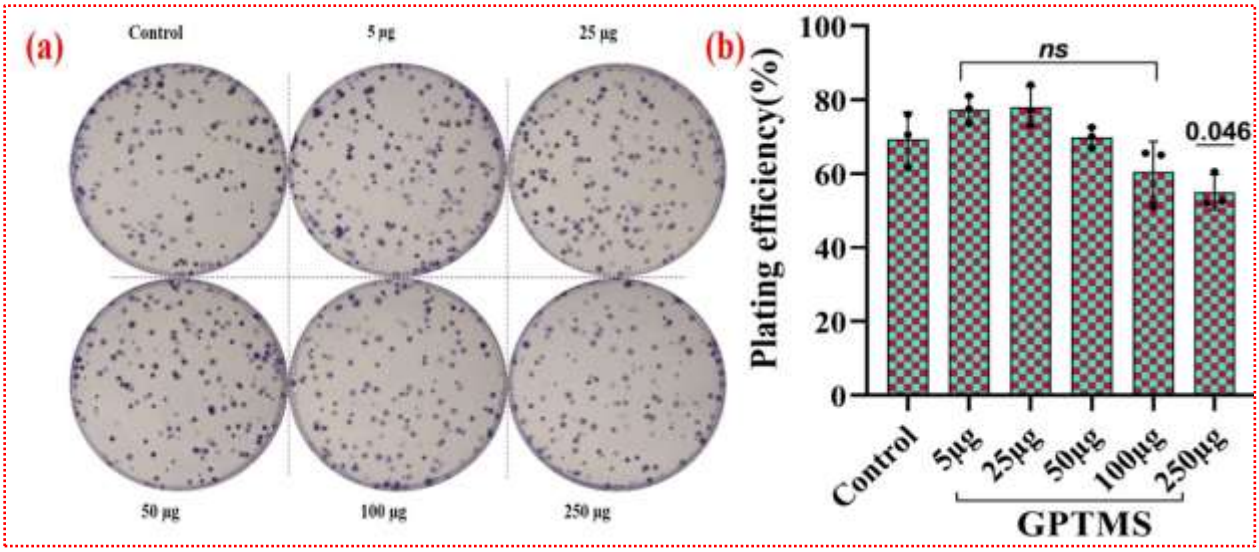

Figure 4B: (a) and (b) Reproductive potential with various concentrations of GPTMS using Macro colony assay.

From the *in-vitro* findings, the relatively non-toxic GPTMS concentrations 5 µg, 25 µg, and 50 µg mL^{-1} were selected for assessment of cellular migration potential. The cells exposed to 5 µg mL^{-1} GPTMS non-significant increase in the migration potential, while the cells treated with 25 µg mL^{-1} and 50 µg mL^{-1} GPTMS showed 2.5 and 1.7 times ($p< 0.5$) increased migration of fibroblasts inside the scratch area respectively. This points toward the higher biocompatibility of GPTMS at a concentration ranging from 5 - 50 µg $mL^{-1,}$ as illustrated in Fig. 4C(a) and (b).

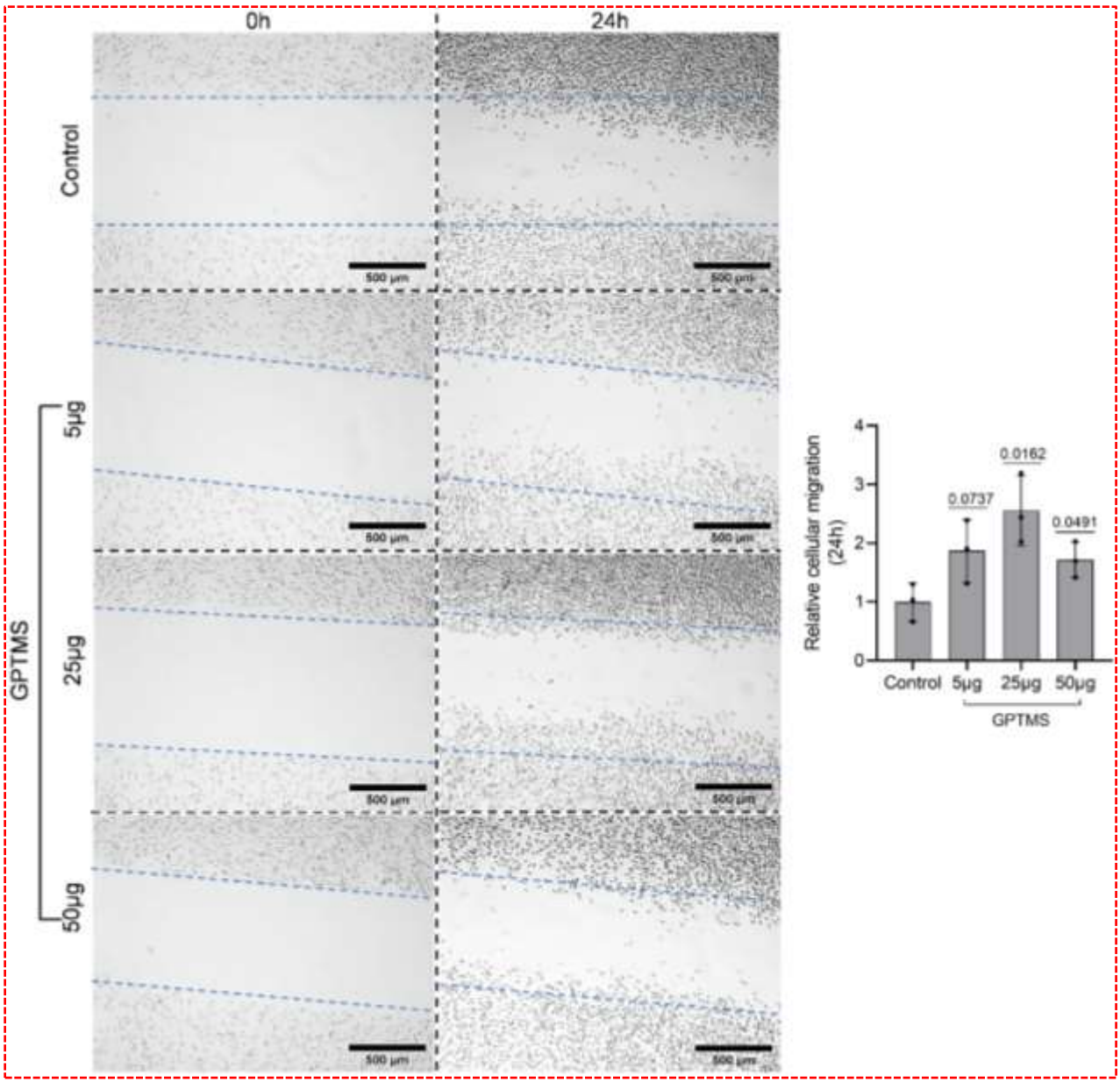

Figure 4C: (a) and (b) Cellular migration potential of GPTMS.

Electrochemical Studies

The electrochemical analysis was performed through CV, DPV, and EIS during the SP17 immunosensor development. The PBS (0.2 M, pH 7.0) consisting of 0.9 % NaCl and 5 mM $[Fe(CN)_6]^{3-/4-}$ as an inner sphere redox species were utilized for whole experiments to monitor the transfer of electrons between the electrolyte and the developed electrodes. The electrons produced from the electrochemical response were transferred through the Fe (III)/Fe (IV) redox mediator leading to a current signal which depicts the distinct role of the developed electrode. This redox species showed a heterogeneous one-electron transmission, i.e., n = 1.

Optimization of analytical parameters

The electrochemical response of the developed immunosensor can be affected by various parameters. Thus, in the present study, for the selection of the ideal binding interactions taking place between SP17 antigens and anti-SP17 antibodies, four distinct parameters such as (i) GPTMS concentration effect, (ii) anti-SP17 antibody concentration, (iii) anti-SP17 antibody incubation time, and (iv) effect of BSA concentration were investigated [the detailed explanation of optimization parameters has been given in supporting information (S1)]. The optimized findings of experimental factors are described in Figure S4 and Table S1 of the supporting information file.

pH study

The pH analysis has a vital significance as pH variations can impact the microstructure and activity of the proteinaceous biological molecules like BSA and Ab immobilized on the surface of the electrode. Therefore, the first electrochemical experiment that was conducted was the effect of pH for exploring the electrochemical analysis of the fabricated BSA/anti-SP17/GPTMS@SAMs/ITO immunoelectrode in PBS (0.2 mM, 0.9 % NaCl) comprising $[Fe(CN)_6]^{3-/4-}$ as redox mediator at 50 mV s^{-1} with varying pH range (6.0 to 8.0). The results showed that the proteinaceous biological molecule's surface charge is based on the buffer solution pH, affecting the electrochemical response, and thus, the maximum anodic current was obtained at neutral pH = 7.0 [Fig. 5(A)]. The attained results depict that the proteinaceous molecule, i.e., the antibody, is reactive in its native form as well as highly stable at pH = 7.0. The alkaline and acidic pH would cause protein denaturation of biological molecules owing involvement of OH^- or H^+ ions on the antibody's amino acids [53][54]. Hence, viewing all these factors, successive electrochemical responses were performed using a PBS buffer of neutral pH.

Electrode study

CV and EIS are efficient methods for providing valuable data on the difference in the current response of the electrode [55]. Due to this, CV and the EIS technique were used to follow the fabrication process of the proposed biosensor and to analyze the interface properties of ITO-modified electrodes. The electrochemical CV studies of the different modified surfaces were investigated at a 50-mV s^{-1} scan rate within a fixed potential window of -0.8 to +0.8 V in 0.2 M PBS comprising the redox species. For all electrodes, a well-defined redox peak current is detected. The peak separation for hydrolyzed bare ITO is more than 400 mV due to a combination of factors, including the surface roughness and heterogeneity of the electrode, the presence of defects and

impurities, and the kinetics of the electrochemical reactions occurring at the electrode surface. As observed in Fig. 5(C), the ITO electrode exhibits an increased value of peak currents at 190.88 μA [curve (i)]. However, low peak currents of 170.56 μA [curve (ii)] were observed after modification with GPTMS (GPTMS@SAMs/ITO) owing to the non-conductive nature of the GPTMS layer. The formation of epoxysilane monolayer was a barrier; therefore, diffusion of redox mediator could not occur to the electrode's surface [42][36]. Moreover, the anti-SP17 antibodies' attachment on the surface of GPTMS@SAMs/ITO instigated mediator-like activity, which increases the transfer of electrons, and thus, an increase in current was seen owing to the small electron tunneling distance between the electrode and antibodies [56]. Therefore, the slight increase in anodic peak currents was recorded at 178.64 μA [curve (iii)]. This also suggests efficient bioconjugation through the Fc region and good orientation of anti-SP17 on the surface of the electrode. Moreover, the electrostatic charge interaction created by Fe^{3-}/Fe^{4-} transformation in the redox probe with the antibody's cationic $-NH_3^+$ terminus (F_{ab} terminal) promotes electron transport across the electrolyte-electrode interface. It may also be inferred that anti-SP17 is immobilized onto the sensor surface without altering their specificity and immunological activity. Then, immobilization of BSA was done by covering the left epoxy ends on the surface of the electrode; hence the electrical conductance decreased drastically to 137.34 μA [curve (iv)] due to the non-conductive property of BSA molecules. This reveals the blockage of unspecific surface sites, which endow the electrode resistant to non-specific adsorption of contaminants and thus resist the permeability of the redox probe $[Fe(CN)_6]^{3-/4-}$ between the electrode surface and the medium. The results show that BSA was immobilized on the anti-SP17/GPTMS@SAMs/ITO electrode.

Further, Electrochemical Impedance Spectroscopy (EIS) studies of ITO, GPTMS@SAMs/ITO, anti-SP17/GPTMS@SAMs/ITO, and BSA/anti-SP17/GPTMS@SAMs/ITO were also performed for characterizing the step-wise modification made on the surface of the ITO electrode in PBS solution containing $[Fe(CN)_6]^{3-/4-}$ in the 100 kHz –10 Hz frequency range at zero (0) potential [Fig. 5(D)]. EIS is an effective way to monitor surface-modified electrode properties and thus allows the understanding of chemical transformation and processes formed on the electrode surface. The semicircle of the Nyquist plot shows the charge transfer resistance (R_{ct}) of various electrodes, which depends on the dielectric features of the electrolyte and the surface of the electrode. Randle's equivalent circuit has been displayed in Fig. S5. Various parameters were estimated, which include time constant (τ), rate constant of heterogeneous electron transfer (K_{ct})

as well as charge transfer resistance (R_{ct}) for ITO, GPTMS@SAMs/ITO, anti-SP17/GPTMS@SAMs/ITO, and BSA/anti-SP17/GPTMS@SAMs/ITO immunoelectrode as described in Table S2 [the detail explained data has been mentioned in Supporting information (S2)]. Moreover, the EIS spectra measurements were also taken in PBS only (pH 7.0) i.e., in the absence of $[Fe(CN)_6]^{3-/4-}$ [Fig. S6] and estimated various parameters (Table S3) to compare the FRA response in PBS having 5mM $[Fe(CN)_6]^{3-/4-}$ and without 5mM $[Fe(CN)_6]^{3-/4-}$. The results of EIS spectra in PBS only showed same trend as EIS spectra in presence of redox species for different modified electrodes, however the semicircle Nyquist plot is not same as in presence of redox species. Thus, the CV results were in agreement with the EIS measurements that revealed the excellent immobilization processes on the electrode surface.

Scan Rate Studies

Interfacial kinetics of the surface of GPTMS@SAMs/ITO and BSA/anti-SP17/ GPTMS@SAMs/ITO electrodes were analyzed by differing the scan rate ranging from 10 to 100 mVs^{-1} [Fig. 5(E) and (F)]. In both cases, the cathodic (Ipc) and anodic (Ipa) peak currents magnitudes rise with the increased value of the scan rate, which shows that the electrochemical process is diffusion control [57][58]. Fig. 5(E) and (F) (upper inset) depict the anodic (Ipa) as well as cathodic (Ipc) peak currents as a function of the square root of the scan rate. Both electrodes illustrate the linear rise in current magnitude with the surge in scan rate values. When performing CV, increasing the scan rate increases the current response observed during the experiment. This is because a faster scan rate allows more redox reactions to occur in a shorter span of time, resulting in a higher current. However, increasing the scan rate also leads to an increase in the peak separation, which refers to the difference in potential between the oxidation and reduction peaks in a CV. This is because as the scan rate increases, the time available for the diffusion of species to the electrode surface decreases. This can lead to a greater separation between the oxidation and reduction peaks as the oxidation and reduction processes become more kinetically controlled. Therefore, increasing the scan rate can result in a trade-off between obtaining a higher current response and maintaining a reasonable peak separation. The full description of this study is provided in the Supporting information (S3).

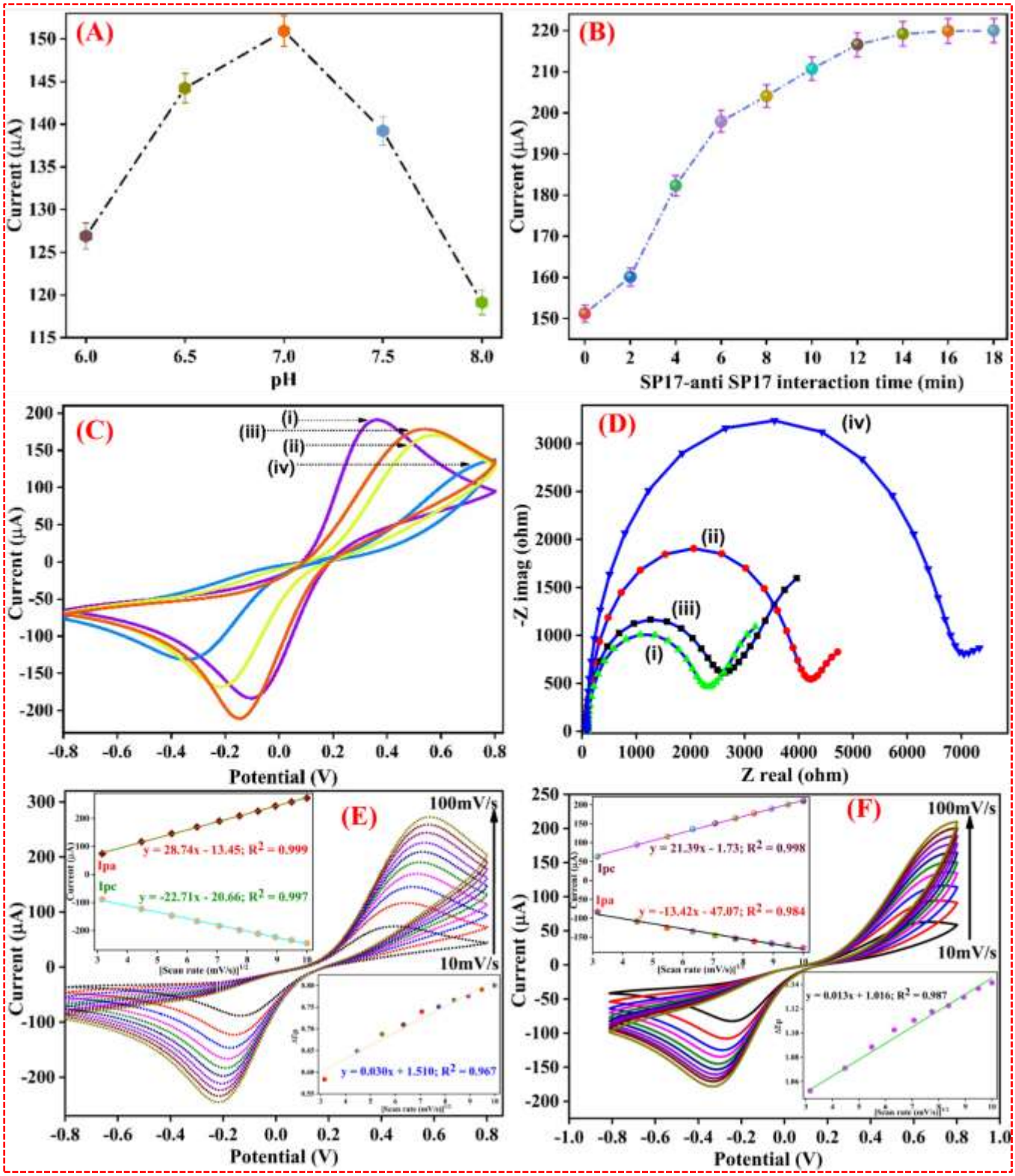

Figure 5. (A) Effect of different pH (6.0-8.0) on BSA/anti-SP17/GPTMS@SAMs/ITO immunoelectrode; (B) Response time studies of BSA/anti-SP17/GPTMS@SAMs/ITO

immunoelectrode as a function of SP17; (C) CV response, and (D) EIS spectra of the step-by-step construction of immunosensor in PBS (0.2 mM; pH 7.0) comprising redox species of hydrolyzed ITO (i), GPTMS@SAMs/ITO (ii), anti-SP17/GPTMS@SAMs/ITO (iii), BSA/anti-SP17/ GPTMS@SAMs/ITO electrodes (iv); CV response of various scan rates from 10 to 100 mVs^{-1}, (E) GPTMS@SAMs/ITO, as well as (F) BSA/anti-SP17/GPTMS@SAMs/ITO immunoelectrode. The upper inset shows the anodic and cathodic peak current magnitude, and the lower inset depicts the difference of oxidation as well as reduction peak potential ($\Delta Ep = Epa - Epc$) versus the square root of scan rate, respectively.

Analytical performance toward SP17 detection

Incubation studies

For monitoring the time needed for completion of interaction between BSA/anti-SP17/GPTMS@SAMs/ITO immunoelectrode with SP17 antigen and for confirming anti-SP17 antibodies-SP17 antigen immunocomplex formation, the incubation analysis was performed by measuring the variations in anodic peak current repeatedly after adding SP17. Here, measurement of BSA/anti-SP17/GPTMS@SAMs/ITO immunoelectrode was done utilizing the CV technique with a particular SP17 concentration, i.e., 4000 pg mL^{-1} intervals for 18 min at 2 min regular. It was seen that after adding a specific concentration, the increase in peak current was reported till 15 min, and after that, flattening of the curve occurs, resulting in saturation of current [Fig. 5(B)]. Thus, 15 min incubation time was given for the complete reaction to occur after adding each concentration of SP17, and therefore, the investigation of the subsequent electrochemical response of the developed immunosensor was done using this procedure.

Electrochemical response studies

To determine the concentration-dependent measurements, the theory of the rate of transportation and charge formation at the surface of the electrode was employed [59]. The analytical response of the developed immunosensor BSA/anti-SP17/GPTMS@SAMs/ITO was conducted by measuring the various SP17 antigens concentrations (100-6000 pg mL^{-1}) under optimum experiment conditions. The electrochemical response of the developed immunosensor was recorded by CV (at 50 mVs^{-1} scan rate within the -0.8V to +0.8V potential range) [Fig. 6A] and DPV (-0.8 to +0.8 V) [Fig. 6C] techniques in PBS solution containing redox species. The charge distribution and diffusion of the redox probe towards the electrode surface vary due to the covalent interaction between antigen and antibody. The variations are because antibodies function as

polyelectrolytes in solution, and their electrical charge changes when they attach to the electrode surface. Thus, these changes are measured by varying the oxidation peak current of CV and DPV by providing a 15 min incubation period. It was established that after increasing the SP17 concentration from 50 to 6000 pg mL^{-1}, there seems to be a linear rise in peak current that got stable after 6000 pg mL^{-1} concentration addition as shown in Fig. 6A and C (the inset displayed the magnified image showing the peak current). The peak current was gradually increased on adding higher concentrations of SP17 is due to the formation of an antigen–antibody complex by probing the features of the interfacial properties. This complex offers additional electroactive locations for unstrained electron transfer at the surface of electrode and results in the formation of electron transfer layer as well as change the conformational structure [60][61][62]. Moreover, the sequence of sperm protein 17 (SP17) antigen (Accession: AAK20878.1, sperm protein 17, Homo sapiens) is known to contain 3 residues of tyrosine (Y) amino acid molecules (full length amino acid sequence has been shown in Fig. S7). During an electrochemical reaction, these tyrosine amino acid molecules undergo oxidation and release electrons resulting in increased peak current as shown in scheme 2 [63,64]. The rise in concentration of tyrosine amino acids due to addition of higher concentrations of SP17 antigen is likely to result in enhanced antigen-antibody interaction onto BSA/anti-SP17/GPTMS@SAMs/ITO immunoelectrode leading to gradual increase in peak currents [9][65]. Alternatively, it may perhaps be attributed to both the conformation changes in the BSA/anti-SP17/GPTMS@SAMs/ITO matrix and the strong affinity of SP17 antigen towards the spatially oriented antibodies that are likely to provide easy conducting paths for electron transfer to the BSA/anti-SP17/GPTMS@SAMs/ITO electrode leading to improved sensing characteristics such as linearity, faster response time and shelf life [66][63,67]. In addition, GPTMS@SAMs get attached to biomolecules covalently (anti-SP17 antibodies and SP17 antigen) as well as act as a molecular wire between the surface of the electrode and biomolecules. Additionally, a similar trend of increased current has been observed for other biological analytes, such as prostate specific antigen [63], carcinoembryonic antigen [68], CYFRA-21-1 (oral cancer biomarker) [65], Aflatoxin B1 [69], Annexin A2 (liver cancer biomarker) [9], SARS-CoV-2 [70], Vibrio cholerae [71], Troponin I[72], S. aureus[73], quinolinic acid (neurotoxin)[74] and influenza virus H1N1 [75], in several label-free electrochemical detection studies.

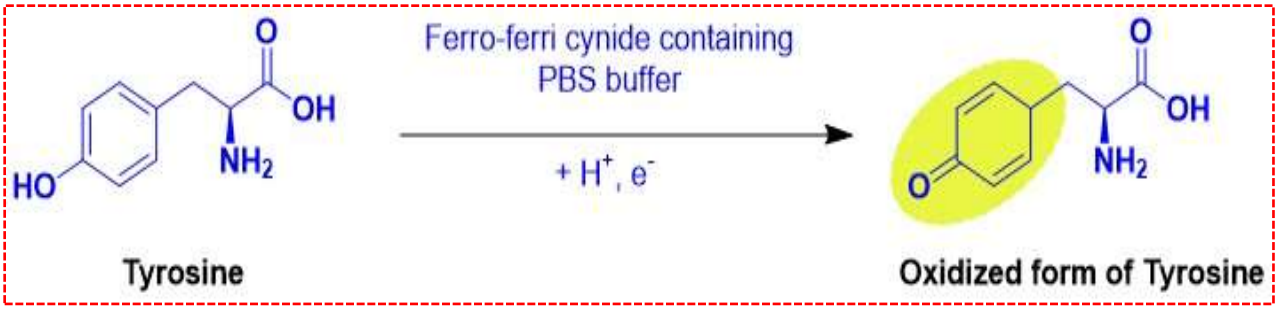

Scheme 2: Schematic illustration of oxidation reaction of Tyrosine molecules.

Moreover, when the concentration of the analyte increases, the potential of the electrode shifts toward a more positive direction [Fig. 6A and C]. This phenomenon is known as the Nernst equation, which relates the electrode potential to the analyte concentration in the solution. The Nernst equation states that the potential difference between the two electrodes in an electrochemical cell is proportional to the logarithm of the ratio of the analyte concentrations at the two electrodes. Specifically, the equation is:

$$E = E0 + (RT/nF) \times \ln([ox]/[red])$$

where: E is the potential difference between the two electrodes; E0 is the standard electrode potential; R is the gas constant; T is the temperature in Kelvin; n is the number of electrons transferred in the electrochemical reaction; F is Faraday's constant; [ox] and [red] are the concentrations of the oxidized and reduced forms of the analyte, respectively.

As the concentration of the analyte increases, the ratio of [ox]/[red] increases, and the logarithmic term in the Nernst equation becomes more positive. Therefore, the overall potential of the electrode shifts in a more positive direction. In summary, the potential of an electrode shifts towards a more positive direction as the concentration of the analyte increases due to the logarithmic relationship described by the Nernst equation.

After optimizing all the experimental parameters, outstanding linearity was achieved between the current difference (ΔI) and SP17 concentration ranging from 50 to 6000 pg mL^{-1}, as depicted in Fig. 6(B and C). The linear curve between peak current as a function of concentrations of SP17 with positive inclination [Fig. 6(B and D)] gave the following linear equation (2) and (3) with a 0.996 and 0.964 linear regression coefficient (R^2).

$Ip = [0.0118\ (\mu A\ mL\ pg^{-1}) \times SP17\ conc.\ (pg\ mL^{-1})] + 171.92\ \mu A,\ R^2 = 0.996$ …….... Eq. (2)

$Ip = [0.0060\ (\mu A\ mL\ pg^{-1}) \times SP17\ conc.\ (pg\ mL^{-1})] + 82.81\ \mu A,\ R^2 = 0.964$ ……. Eq. (3)

The SAMs of GPTMS acted as the outstanding matrix due to the strong non-covalent interactions with the biological molecules having the negative surface charge, which helped in adsorbing the mass anti-SP17 antibodies, therefore achieving a remarkable 0.047 μA mL pg^{-1} cm^{-2} and 0.024 μA mL pg^{-1} cm^{-2} sensitivity along with R^2 of 0.996 and 0.964 as well as the rapid response time of 15 min through CV and DPV, respectively. The sensitivity was calculated from the linear plot' slope/surface area, i.e., 0.25 cm^2. The immunosensor depicted a broad linear detection range (LDR) for SP17 from 100 pg mL^{-1} to 6000 pg mL^{-1} (CV) and 50-5500 pg mL^{-1} (DPV). The limit of quantification (LOQ) and the detection limit was estimated as 158.58 pg mL^{-1} (CV) and 476.35 pg mL^{-1} (DPV) (calculated using= 10σ/m) and 47.57 pg mL^{-1} (CV) and 142.9 pg mL^{-1} (DPV) (calculated using= 3σ/m), respectively, where m depicts the sensitivity, as well as σ, shows the standard deviation of intercept [76]. Henceforth, the developed GPTMS@SAMs biosensor exhibits outstanding biosensing parameters for effectively determining SP17. Table 1A represents the comparative parameters of an earlier published biosensor for detecting SP17. The BSA/anti-SP17/GPTMS@SAMs/ITO immunosensor shows improved sensitivity, LDR value, and response time than our previously reported work [7] (0.013 μA mL pg^{-1} cm^{-2}; 100-6000 pg mL^{-1} and 15 min, respectively) and ELISA kit (64–2400 pg mL^{-1}). GPTMS-SAMs have one molecule thick layer as well as offer facile contact to the SP17 antigen for rapid charge transfer owing to the molecular interaction between the biomolecules in the vicinity of the surface of electrode and analyte, thus leading to broad LDR from 50 to 6000 pg mL^{-1} and low LOD of 47.57 pg mL^{-1}. From this outstanding detection limit, the immunosensor can sense 22×10^7 SP17 molecules [detailed calculation for SP17 molecules has been given in supplementary information, S4], hence determining an ultralow SP17 concentration.

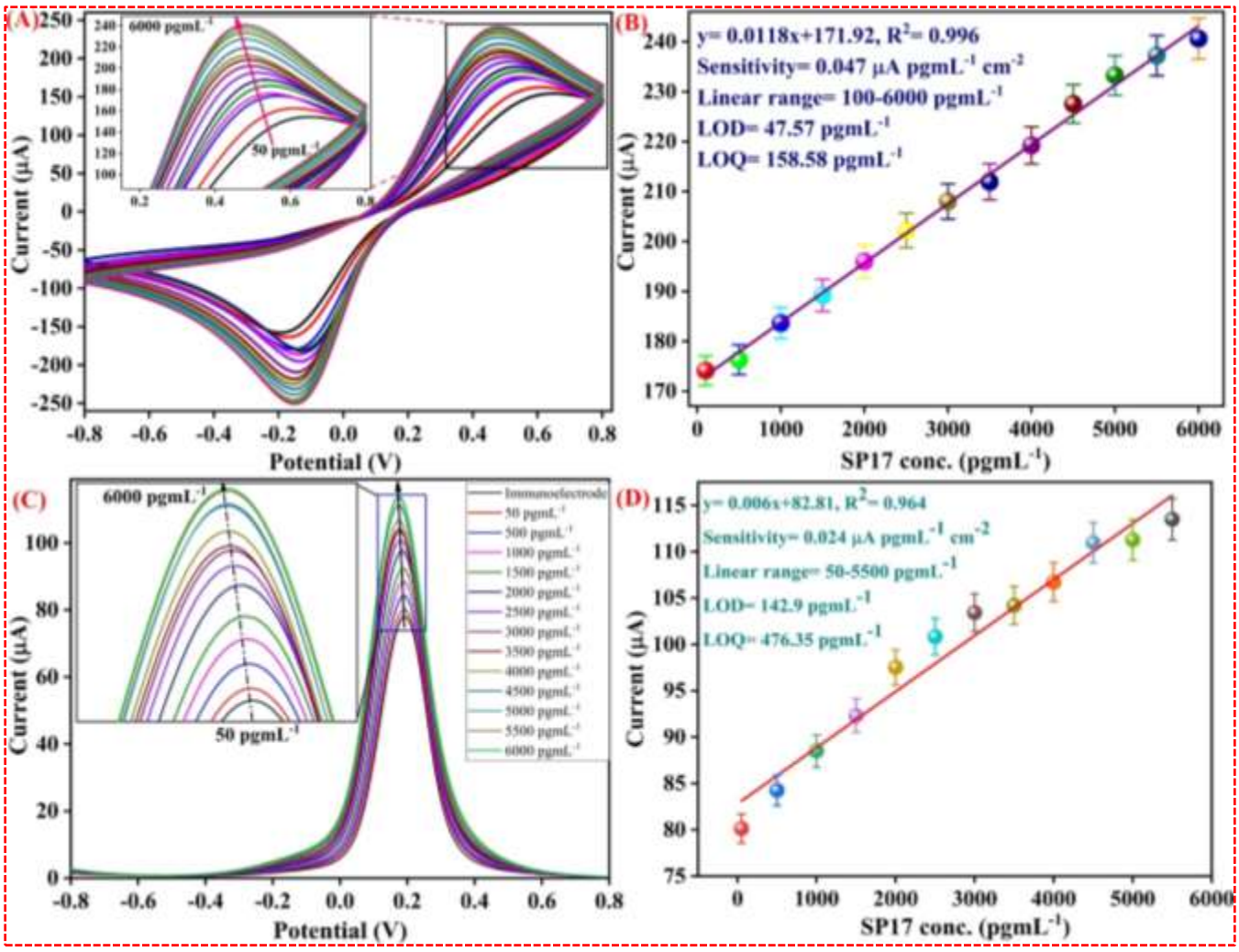

Figure 6. The electrochemical response of BSA/anti-SP17/GPTMS@SAMs/ITO immunoelectrode as a function of increasing concentrations of SP17 (50–6000 pg mL^{-1}) through (A) CV and (C) DPV techniques and calibration plot of magnitude of anodic peak current against concentration of SP17 through (B) CV (50–6000 pg mL^{-1}) and (D) DPV (50-5500 pg mL^{-1}) techniques [inset shows the magnified image].

Table 1A. Comparative biosensing parameters of earlier reported biosensors for SP17 detection.

Immunoelectrode	Method	Sensitivity (µA $mL^{-1}pg^{-1}$ cm^{-2})	Linear range (pg mL^{-1})	LOD (pg mL^{-1})	LOQ (pg mL^{-1})	Response Time (min)	Regeneration	Shelf-life (week)	Ref.
BSA/anti-SP-17/APTMS/ITO	DPV	0.013	100-5000	70.07	233.57	30	5 (90%)	5	[7]
BSA/anti-SP17/GPTMS@SAMs/ITO	CV	0.047	100-6000	47.57	158.58	15	5 (95%)	8	**Present work**
	DPV	0.024	50-5500	142.9	476.35				

Further, the estimation of the association constant, i.e., K_a, was done using the Hens-Wolf plot, which is between the concentration of SP17 and SP17 conc./current for BSA/anti-SP17/GPTMS@SAMs/ITO immunoelectrode as depicted in Fig. 7(a) and the calculated value obtained is 250 pg mL^{-1}. K_a depends on various factors of the developed immunosensor, such as how immobilization of antibodies on the surface of the electrode was done and biomolecules binding areas, that could be the basis of different conformation variations in the structure of antibodies present on the electrode surface. The increased K_a value shows increased BSA/anti-SP17/GPTMS@SAMs/ITO immunoelectrode affinity for SP17 owing to the higher loading and constructive anti-SP17 conformation on the surface of the electrode. The value of K_a was estimated through the inverse slope values achieved from the Hanes-Wolf linear fitting plot.

Control study

Using the CV technique, a control study was performed to determine the SP17 concentrations' effect on the electrochemical response of the GPTMS@SAMs/ITO electrode. It was observed from Fig. 7(b) those negligible variations occurred in anodic peak current against the increasing values of antigen SP17 concentrations from 100 to 6000 pg mL^{-1}. Thus, it was concluded that the fabrication of immunocomplex between anti-SP17 antibodies and SP17 antigen is entirely responsible for the difference in peak current during the electrochemical response study and not because of the interaction between GPTMS@SAMs/ITO and SP17 molecules.

Selectivity studies

Further, selectivity is the standard demand for developing an immunosensor. For evaluating the selectivity/interference of the developed platform towards SP17, some analogous proteins and metabolites [cytokeratin 19 fragment (CYFRA-2-1), TNF-α, uric acid, oxalic acid, ascorbic acid, interleukin-8 (IL-8), urea, and glucose] present in human serum were selected as interference biomarkers. These biomarkers are successively added to measure the electrochemical response of BSA/anti-SP17/GPTMS@SAMs/ITO immunoelectrode. As seen from Fig. 7(c), the difference in current occurred only after SP17 addition. This is caused owing to the specific recognition between SP17 antigen and anti-SP17 antibody, as no variation was seen on adding other interferents. Therefore, the fabricated biosensor depicted high selectivity for the detection of SP17. Furthermore, the interference from analytes is estimated using Eq. (4) to calculate the selectivity coefficient (SC).

$$SC = \frac{I_{c+i}}{I_c} \text{.....} \quad \text{(Eq.4)}$$

Where Ic and (Ic + i) correspond to the current value in the presence of SP17 and interfering molecules, respectively. The calculated SC for the tested analytes is found to be significantly low (SC ~ 1), indicating the minimal effect of the interfering molecules on the immunosensor response.

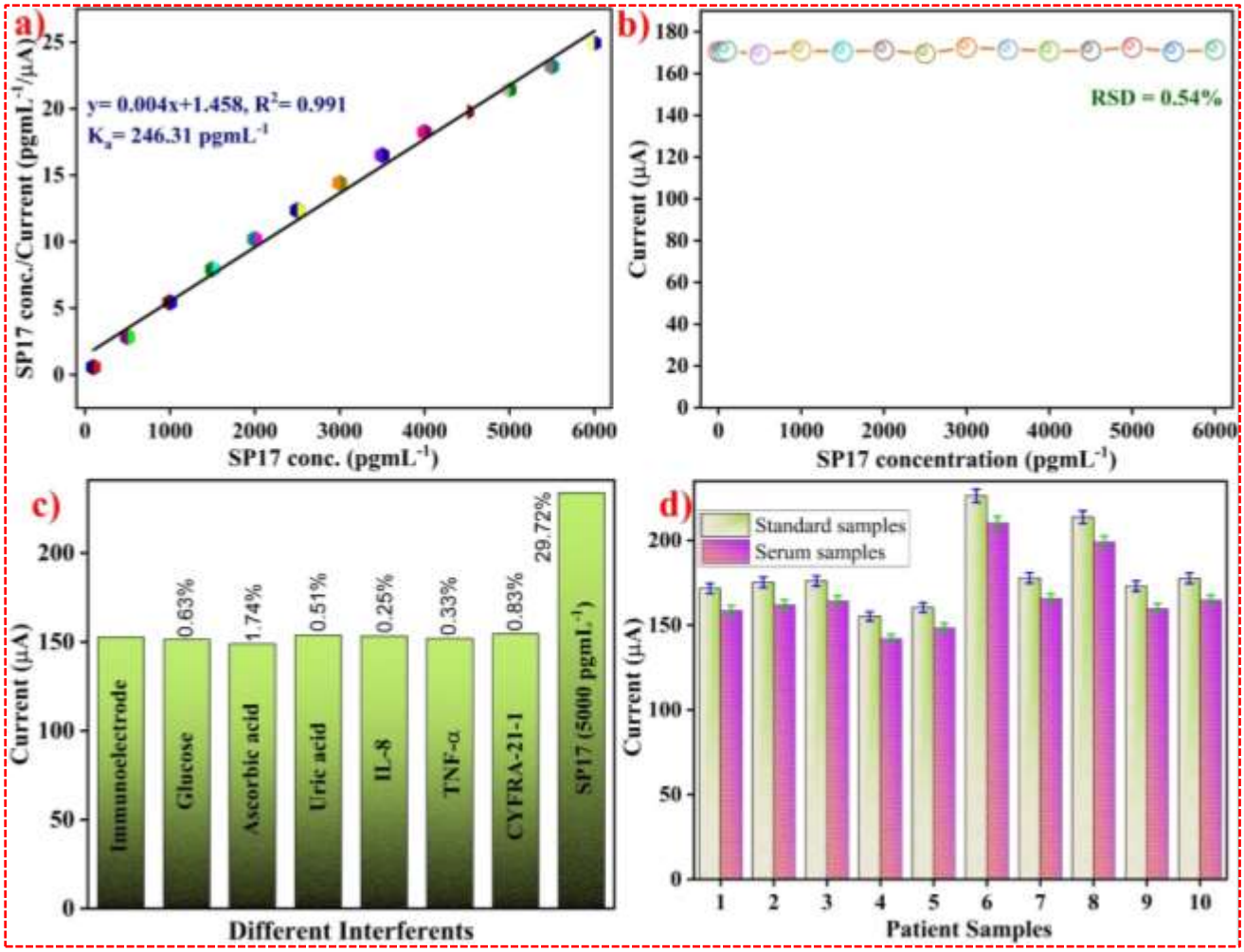

Figure 7: (a) Measurement of Ka value using Hens-Wolf plot from developed biosensor; (b) Control studies depicting the electrochemical response of GPTMS@SAMs/ITO as a function of SP17 concentrations (100 pg mL^{-1}- 6000 pg mL^{-1}), (c) Selectivity response performed utilizing the different analytes present in the blood of human in addition to SP17; and (d) Current comparison depicted by bar graph obtained using the CV of cancer patient samples and standard response.

Reusability, reproducibility, repeatability, and shelf-life studies

Repeatability and reproducibility are two main parameters of immunosensors development for practical utility. To observe the reproducibility response of the fabricated immunosensor, 8 diverse

electrodes were fabricated independently under similar experimental situations and used for evaluating the peak current response. The low relative standard deviation (RSD) was found at 3.42 %, as illustrated in Fig. 8(A). In addition, the repeatability of the proposed BSA/anti-SP17/GPTMS@SAMs/ITO immunoelectrode was assessed by taking 6 successive measurements for a specific SP17 concentration (6000 pg mL^{-1}) employing the CV technique [Fig. 8(B)]. A negligible difference in current was seen for repeatability with a % RSD of 0.93 %, which is quite acceptable. Both these results depicted capability and fair precision for providing repeatable and reproducible results.

In order to study the regeneration response of the immunosensor, the developed electrode was dipped in an acidic solution (HCl, 0.1 %, and ultra-pure water) after coupling of SP17 antigen, as well as again measuring the reading. The immunosensor electrochemical responses were recorded after each regeneration procedure. As depicted in Fig. 8(C), the BSA/anti-SP17/ GPTMS@SAMs/ITO immunosensor could be reutilized at least 5 times as 95 % retention of initial response was reported.

The long shelf-life is vital for its application as a biosensor. Thus, the shelf life of developed BSA/anti-SP17/GPTMS@SAMs/ITO immunoelectrode was measured in PBS (pH 7.0) at one-week intervals through CV analysis for 11 consecutive weeks [Fig. 8(D)]. The immunoelectrode depicts a 90 % response for 8 weeks, after which decrement of the peak current occurred abruptly. Hence, the obtained shelf-life of immunoelectrode was 6 weeks when kept at 4 °C.

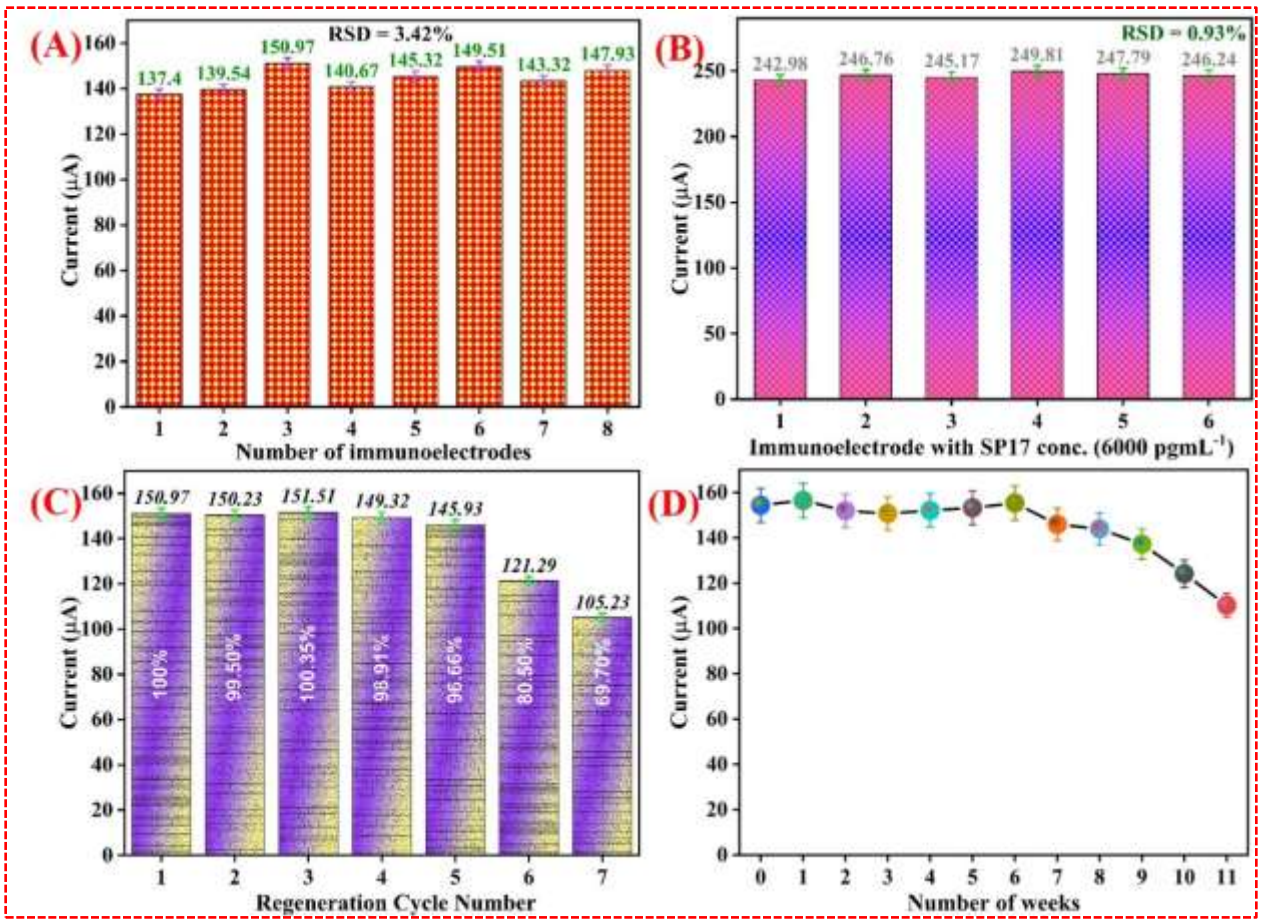

Figure 8. Reproducibility (A) and Repeatability (B) examination of BSA/anti-SP17/GPTMS@SAMs /ITO immunoelectrode, respectively. Regeneration signal study of the BSA/anti-SP17/GPTMS@SAMs/ITO immunoelectrode (C); and Stability study of the fabricated SP17/GPTMS@SAMs/ITO immunoelectrode (D).

Practical application in human blood samples

The practical utility of the immunosensor is vital for analyzing human biological samples [77][78]. SP17 is regarded as a tumor biomarker in an individual's serum; thus, SP17 concentration determination in the blood is vital. For this experiment, GPTMS@SAMs modified immunoelectrode was used to detect SP17 concentration in a complex biological medium, i.e., human blood samples. We obtained ten serum samples of cancerous patients with swelling or lesions in the mouth produced by tobacco consumption over many years to determine SP17antigen. We quantified the concentration of SP17 through a quantitative sandwich ELISA kit (CUSABIO; Catalog No.- CSB-EL022451HU) and repeated it thrice. The wells of microtiter were pre-covered with FITC anti-SP17 antibody. After following all the steps according to manual instructions, a

colorimetric reaction took place, and its absorbance at 450 nm was recorded in an ELISA plate reader. A sequence of SP17 concentration in blood samples found by ELISA was utilized for testing the accuracy of the developed biosensor.

After the quantification was done, incubation for 15 min was given to the blood samples, and the electrochemical response *via* CV method was checked for the fabricated BSA/anti-SP17/GPTMS@SAMs/ITO immunoelectrode. It was found that the peak current value measured for the real blood samples matched the standard concentration's current. We saw a brilliant co-relation between the CV current magnitude achieved for standard concentrations of SP17 and concentrations of SP17 in a real blood sample obtained *via* ELISA [Fig. 7(d)]. The observed results revealed ≤10% of %RSD, indicating high accuracy of the fabricated biosensor that could detect the SP17 in human blood samples. Also, 97.89 % to 99.37 % (Table 1B) recovery rates were obtained that are quite satisfactory. Additionally, recovery results depict developed immunosensor robustness in examining the human blood samples. The developed immunosensor is a sensitive, reusable, and low-cost technique, while the ELISA needs a lengthy application procedure and is high-cost. Thus, the utilization of biosensors is more beneficial as compared to the ELISA kits.

Table 1B. Quantification of SP17 protein present in the serum of cancer patients through ELISA and its validation utilizing the developed BSA/anti-SP17/GPTMS@SAMs/ITO immunosensor.

S. No.	Sp17 concentration determined using ELISA (in pg mL^{-1})	Peak current (μA) obtained for standard Sp17 samples	Peak current (μA) obtained with Patients seum samples	% RSD	% recovery
1.	58.94	171.63	168.93	1.12%	98.42
2.	206.74	175.32	172.29	1.23%	98.27
3.	336.97	176.12	175.02	0.443%	99.37
4.	25.26	155.23	151.97	1.5%	97.89
5.	52.21	160.45	157.97	1.1%	98.45
6.	4480.41	226.38	223.93	0.769%	98.91
7.	450.50	177.92	176.32	0.639%	99.10
8.	3677.62	213.78	211.92	0.618%	99.12
9.	275.2	173.07	170.12	1.22%	98.29
10.	523.96	177.71	175.29	0.97%	98.63

STATISTICAL ANALYSIS

All bar plots show error bars and the arithmetic mean. Individual dots represent an average of experimental replicates. Unless noted, each experiment had three replicates (n=3). A two-tailed Student t-test with GraphPad Prism8 was used to analyze the data. Results with p values <0.05 were significantly considered.

To verify the assay accuracy, coefficients of variation (CoV) and intra-test standard deviations (SD) at different SP17 standard concentrations were evaluated using the CV technique (100-6000 pg mL^{-1}). The studies were repeated thrice (n = 3), and three successive measurements were obtained after a specified optimal incubation period on a single day. As a result, the CoV was calculated using an average of three or nine observations. CV methods determined the entire mean intra-assay CoV (%) to be 0.06%. The reported mean intra-assay CoV (%) values depict increased assay accuracy for clinical uses. Furthermore, for validating the results received using cancer patients' blood samples, the statistical examination was done employing students' F-test and t-test by associating its reaction with the electrochemical behavior of standard electrodes, i.e., BSA/anti-SP17/GPTMS@SAMs/ITO. To do this, the average of anodic current of at least ten standard electrodes was measured before as well as after adding the serum samples, and every reading was taken thrice (n = 10×3). The paired t-test revealed a significant statistical variation within a 99.9% (p 0.001) confidence interval between the two currents, suggesting that the variations did not attribute to arbitrary mistakes. Moreover, the F-test revealed a significant difference in the electrochemical response of standard electrodes before as well as after adding the blood samples, having p 0.001. These findings show that our manufactured immunosensor can accurately detect SP17 in cancer patients' serum samples.

CONCLUSION

In summary, we fabricated a highly sensitive, selective, and reusable immunosensor for SP17 antigen detection in a human serum sample for the first time *via* GPTMS@SAMs modified low-cost and disposable ITO biosensing platform. For designing the immunosensor, anti-SP17 antibodies, as well as GPTMS@SAMs, were used as biorecognition molecules and immobilization matrices, respectively. The use of the GPTMS@SAMs provides the transfer of electrons between the working electrode surface and electrolyte and delivers binding sites for anti-SP17 bioreceptors. The proposed immunosensor depicts many benefits like simple, repeatability, selectivity, good reproducibility, low LOD (47.57 & 142.9 pg mL^{-1}), wide linear detection range (100-6000 & 50-

5500 pg mL^{-1}), improved sensitivity (0.013 & 0.024 μA mL pg^{-1} cm^{-2}) by CV as well as DPV for detecting SP17 antigen. Additionally, the immunoelectrode could be repeated 5 times for the subsequent determination. These results provide a simple, stable, and reusable amperometric technique developed for SP17 detection, which will help in the early diagnosis of a cancer biomarker in real samples. This immunosensor can be used for widespread detection strategy for SP17 detection in the future. Moreover, the safety and biocompatibility of the GPTMS were in good agreement with the MTT assay findings, demonstrating the excellent efficacy of the GPTMS materials to be employed as the core electrode material for the futuristic fabrication of a biocompatible biosensing platform.

IMPACT OF THE RESEARCH IN THE ADVANCEMENT OF KNOWLEDGE OR BENEFIT TO MANKIND

The main objective of this paper is fabrication of nanotechnology based cost-effective and highly efficient electrochemical biosensors for cancer biomarker detection which will help in early diagnosis of cancer biomarker in real samples. Even though many researchers were worked on the development of biosensors for cancer biomarker detection, the present study fabricates an ultra-sensitive, stable, regenerative, and novel immunosensor for a new type of cancer biomarker known as sperm protein 17 (SP17) using self-assembled monolayers (SAMs) of 3-glycidoxypropyltrimethoxysilane (GPTMS) for the first time with high sensitivity and low limit of detection.

Non-invasive detection of cancer biomarkers in real samples provides an additional benefit to a biosensor that aids in overcoming the limitations of other traditional diagnostic methods. The proposed diagnostic sensing platform would permit SP17 cancer biomarker determination in the initial stage and significantly contribute to clinical laboratories. In addition, the developed biosensor will help medical professionals to have a check on the alarming rate of cancer because biosensors exhibit exceptional performance capabilities like high sensitivity and specificity and rapid response. Non-invasive detection of cancer biomarkers in real samples provide an extra advantage to biosensor that help to overcome the limitations of other conventional diagnostic techniques. The developed diagnostic sensing interface would allow SP17 cancer biomarker detection in early stage and would be a great contribution in clinical laboratories.

In addition, for the first time, the GPTMS were examined for its cytotoxicity in human lymphocyte cells using hemolysis and biocompatibility utilizing various *in vitro* studies in murine fibroblast

cell line L929, demonstrating the excellent efficacy of the GPTMS materials to be employed as the core electrode material for the futuristic application in nanoelectronics, *in vivo* investigations, as well as flexible wearables.

LITERATURE REFERENCES

[1] M. Piñeros, L. Mery, I. Soerjomataram, F. Bray, E. Steliarova-Foucher, Scaling up the surveillance of childhood cancer: a global roadmap, JNCI J. Natl. Cancer Inst. 113 (2021) 9–15.

[2] M. Pourmadadi, H. Soleimani Dinani, F. Saeidi Tabar, K. Khassi, S. Janfaza, N. Tasnim, M. Hoorfar, Properties and Applications of Graphene and Its Derivatives in Biosensors for Cancer Detection: A Comprehensive Review, Biosensors. 12 (2022) 269.

[3] H. Sung, J. Ferlay, R.L. Siegel, M. Laversanne, I. Soerjomataram, A. Jemal, F. Bray, Global cancer statistics 2020: GLOBOCAN estimates of incidence and mortality worldwide for 36 cancers in 185 countries, CA. Cancer J. Clin. 71 (2021) 209–249.

[4] D. Ou, D. Sun, X. Lin, Z. Liang, Y. Zhong, Z. Chen, A dual-aptamer-based biosensor for specific detection of breast cancer biomarker HER2 via flower-like nanozymes and DNA nanostructures, J. Mater. Chem. B. 7 (2019) 3661–3669.

[5] A.C. Pereira, M.G.F. Sales, L.R. Rodrigues, Biosensors for rapid detection of breast cancer biomarkers, in: Adv. Biosens. Heal. Care Appl., Elsevier, 2019: pp. 71–103.

[6] X.Y. Wang, Y.G. Feng, A.J. Wang, L.P. Mei, P.X. Yuan, X. Luo, J.J. Feng, A facile ratiometric electrochemical strategy for ultrasensitive monitoring HER2 using polydopamine-grafted-ferrocene/reduced graphene oxide, Au@Ag nanoshuttles and hollow Ni@ PtNi yolk-shell nanocages, Sensors Actuators B Chem. 331 (2021) 129460.

[7] A.K. Yadav, P. Gulati, R. Sharma, A. Thakkar, P.R. Solanki, Fabrication of alkoxysilane substituted polymer-modified disposable biosensing platform: Towards sperm protein 17 sensing as a new cancer biomarker, Talanta. 243 (2022) 123376.

[8] C. Zhou, D. Liu, L. Xu, Q. Li, J. Song, S. Xu, R. Xing, H. Song, A sensitive label–free amperometric immunosensor for alpha-fetoprotein based on gold nanorods with different aspect ratio, Sci. Rep. 5 (2015) 1–7.

[9] D. Chauhan, Y. Kumar, R. Chandra, S. Kumar, 2D transparent few-layered hydrogen substituted graphdiyne nano-interface for unprecedented ultralow ANXA2 cancer biomarker detection, Biosens. Bioelectron. (2022) 114433.

[10] M. Aydın, E.B. Aydın, M.K. Sezgintürk, Electrochemical immunosensor for CDH22 biomarker based on benzaldehyde substituted poly (phosphazene) modified disposable ITO electrode: A new fabrication strategy for biosensors, Biosens. Bioelectron. 126 (2019) 230–239.

[11] A. Kumar, B. Purohit, P.K. Maurya, L.M. Pandey, P. Chandra, Engineered nanomaterial assisted signal-amplification strategies for enhancing analytical performance of electrochemical biosensors, Electroanalysis. 31 (2019) 1615–1629.

[12] P. Chandra, R. Prakash, Nanobiomaterial engineering, Springer, 2020.

[13] K. Mahato, A. Prasad, P. Maurya, P. Chandra, Nanobiosensors: next generation point-of-care biomedical devices for personalized diagnosis, J. Anal. Bioanal. Tech. 7 (2016).

[14] J.M. Moon, D.M. Kim, M.H. Kim, J.Y. Han, D.K. Jung, Y.B. Shim, A disposable amperometric dual-sensor for the detection of hemoglobin and glycated hemoglobin in a finger prick blood sample, Biosens. Bioelectron. 91 (2017) 128–135.

[15] S. Chung, J.M. Moon, J. Choi, H. Hwang, Y.B. Shim, Magnetic force assisted electrochemical sensor for the detection of thrombin with aptamer-antibody sandwich formation, Biosens. Bioelectron. 117 (2018) 480–486.

[16] A.C. Sun, D.A. Hall, Point-of-care smartphone-based electrochemical biosensing, Electroanalysis. 31 (2019) 2–16.

[17] H. Zeng, D.A.Y. Agyapong, C. Li, R. Zhao, H. Yang, C. Wu, Y. Jiang, Y. Liu, A carcinoembryonic antigen optoelectronic immunosensor based on thiol-derivative-nanogold labeled anti-CEA antibody nanomaterial and gold modified ITO, Sensors Actuators B Chem. 221 (2015) 22–27.

[18] A.K. Yadav, D. Verma, P.R. Solanki, Electrophoretically deposited L-cysteine functionalized MoS_2@MWCNT nanocomposite platform: a smart approach toward highly sensitive and label-free detection of gentamicin, Mater. Today Chem. 22 (2021) 100567. https://doi.org/10.1016/J.MTCHEM.2021.100567.

[19] A.K. Yadav, D. Verma, G. Lakshmi, S. Eremin, P.R. Solanki, Fabrication of label-free and ultrasensitive electrochemical immunosensor based on molybdenum disulfide nanoparticles modified disposable ITO: An analytical platform for antibiotic detection in food samples, Food Chem. 363 (2021) 130245.

[20] D. Chauhan, A.K. Yadav, P.R. Solanki, Carbon cloth-based immunosensor for detection of

25-hydroxy vitamin D 3, Microchim. Acta. 188 (2021) 1–11.

[21] A.K. Yadav, P. Gulati, R. Sharma, A. Thakkar, P.R. Solanki, Fabrication of alkoxysilane substituted polymer-modified disposable biosensing platform: Toward sperm protein 17 sensing as a new cancer biomarker, Talanta. (2022) 123376.

[22] S.K. Mishra, A.K. Srivastava, D. Kumar, A. Mulchandani, Protein functionalized Pt nanoparticles-conducting polymer nanocomposite film: characterization and immunosensor application, Polymer (Guildf). 55 (2014) 4003–4011.

[23] C.M. Pandey, S. Dewan, S. Chawla, B.K. Yadav, G. Sumana, B.D. Malhotra, Controlled deposition of functionalized silica coated zinc oxide nano-assemblies at the air/water interface for blood cancer detection, Anal. Chim. Acta. 937 (2016) 29–38.

[24] D. Verma, A.K. Yadav, M. Das Mukherjee, P.R. Solanki, Fabrication of a sensitive electrochemical sensor platform using reduced graphene oxide-molybdenum trioxide nanocomposite for BPA detection: An endocrine disruptor, J. Environ. Chem. Eng. 9 (2021) 105504.

[25] M. Aydın, E.B. Aydın, M.K. Sezgintürk, A highly selective poly (thiophene)-graft-poly (methacrylamide) polymer modified ITO electrode for neuron specific enolase detection in human serum, Macromol. Biosci. 19 (2019) 1900109.

[26] L.Y.S. Lee, T.C. Sutherland, S. Rucareanu, R.B. Lennox, Ferrocenylalkylthiolates as a probe of heterogeneity in binary self-assembled monolayers on gold, Langmuir. 22 (2006) 4438–4444.

[27] D. Samanta, A. Sarkar, Immobilization of bio-macromolecules on self-assembled monolayers: methods and sensor applications, Chem. Soc. Rev. 40 (2011) 2567–2592.

[28] G. Demirel, Z. Rzaev, S. Patir, E. Pişkin, Poly (N-isopropylacrylamide) layers on silicon wafers as smart DNA-sensor platforms, J. Nanosci. Nanotechnol. 9 (2009) 1865–1871.

[29] S.M. Lee, H.J. Cho, J.Y. Han, H.J. Yoon, K.H. Lee, D.H. Jeong, Y.S. Lee, Silver nanoparticles preferentially reduced on PEG-grafted glass surfaces for SERS applications, Mater. Res. Bull. 48 (2013) 1523–1529.

[30] J.H.T. Luong, K.B. Male, J.D. Glennon, Biosensor technology: technology push versus market pull, Biotechnol. Adv. 26 (2008) 492–500.

[31] L. Yang, Y. Li, AFM and impedance spectroscopy characterization of the immobilization of antibodies on indium–tin oxide electrode through self-assembled monolayer of

epoxysilane and their capture of Escherichia coli O157: H7, Biosens. Bioelectron. 20 (2005) 1407–1416.

[32] Y. Rai, R. Pathak, N. Kumari, D.K. Sah, S. Pandey, N. Kalra, R. Soni, B.S. Dwarakanath, A.N. Bhatt, Mitochondrial biogenesis and metabolic hyperactivation limits the application of MTT assay in the estimation of radiation induced growth inhibition, Sci. Rep. 8 (2018). https://doi.org/10.1038/s41598-018-19930-w.

[33] I. Gupta, A. Kumar, A.N. Bhatt, S. Sapra, S. Gandhi, Green synthesis-mediated silver nanoparticles based biocomposite films for wound healing application, J. Inorg. Organomet. Polym. Mater. 32 (2022) 2994–3011.

[34] A.N. Bhatt, A. Kumar, Y. Rai, N. Kumari, D. Vedagiri, K.H. Harshan, V. Chinnadurai, S. Chandna, Glycolytic inhibitor 2-Deoxy-D-glucose attenuates SARS-CoV-2 multiplication in host cells and weakens the infective potential of progeny virions, Life Sci. 295 (2022) 120411.

[35] A. Kumar, D.K. Sah, K. Khanna, Y. Rai, A.K. Yadav, M.S. Ansari, A.N. Bhatt, A calcium and zinc composite alginate hydrogel for pre-hospital hemostasis and wound care, Carbohydr. Polym. 299 (2023) 120186.

[36] S. Kumar, J. Singh, V. V Agrawal, M. Ahamad, B.D. Malhotra, Biocompatible self-assembled monolayer platform based on (3-glycidoxypropyl) trimethoxysilane for total cholesterol estimation, Anal. Methods. 3 (2011) 2237–2245.

[37] A.K. Yadav, T.K. Dhiman, G. Lakshmi, A.N. Berlina, P.R. Solanki, A highly sensitive label-free amperometric biosensor for norfloxacin detection based on chitosan-yttria nanocomposite, Int. J. Biol. Macromol. 151 (2020) 566–575.

[38] G. Lakshmi, A.K. Yadav, N. Mehlawat, R. Jalandra, P.R. Solanki, A. Kumar, Gut microbiota derived trimethylamine N-oxide (TMAO) detection through molecularly imprinted polymer based sensor, Sci. Rep. 11 (2021) 1–14.

[39] J.M. Antonucci, S.H. Dickens, B.O. Fowler, H.H.K. Xu, W.G. McDonough, Chemistry of silanes: interfaces in dental polymers and composites, J. Res. Natl. Inst. Stand. Technol. 110 (2005) 541.

[40] Y. Gu, C.C. Chen, Eliminating the interference of oxygen for sensing hydrogen peroxide with the polyaniline modified electrode, Sensors. 8 (2008) 8237–8247.

[41] P. Khullar, J. V Badilla, R.G. Kelly, The Use of a Sintered Ag/AgCl Electrode as Both

Reference and Counter Electrode for Electrochemical Measurements in Thin Film Electrolytes, ECS Electrochem. Lett. 4 (2015) C31.

[42] N. Yılmaz, E.B. Aydın, M.K. Sezgintürk, An epoxysilane modified indium tin oxide electrode for the determination of PAK 2: application in human serum samples, Anal. Chim. Acta. 1062 (2019) 68–77.

[43] E.B. Aydın, M. Aydın, M.K. Sezgintürk, Construction of succinimide group substituted polythiophene polymer functionalized sensing platform for ultrasensitive detection of KLK 4 cancer biomarker, Sensors Actuators B Chem. 325 (2020) 128788.

[44] F.G.L.M. Borsagli, V.S.T. Ciminelli, C.L. Ladeira, D.J. Haas, A.P. Lage, H.S. Mansur, Multi-functional eco-friendly 3D scaffolds based on N-acyl thiolated chitosan for potential adsorption of methyl orange and antibacterial activity against Pseudomonas aeruginosa, J. Environ. Chem. Eng. 7 (2019) 103286.

[45] B. Riegel, S. Blittersdorf, W. Kiefer, S. Hofacker, M. Müller, G. Schottner, Kinetic investigations of hydrolysis and condensation of the glycidoxypropyltrimethoxysilane/aminopropyltriethoxy-silane system by means of FT-Raman spectroscopy I, J. Non. Cryst. Solids. 226 (1998) 76–84.

[46] I.M. Šapić, L. Bistričić, V. Volovšek, V. Dananić, K. Furić, DFT study of molecular structure and vibrations of 3-glycidoxypropyltrimethoxysilane, Spectrochim. Acta Part A Mol. Biomol. Spectrosc. 72 (2009) 833–840.

[47] M. Aydın, E.B. Aydın, M.K. Sezgintürk, A highly selective electrochemical immunosensor based on conductive carbon black and star PGMA polymer composite material for IL-8 biomarker detection in human serum and saliva, Biosens. Bioelectron. 117 (2018) 720–728.

[48] F.G.L.M. Borsagli, I.C. Carvalho, H.S. Mansur, Amino acid-grafted and N-acylated chitosan thiomers: Construction of 3D bio-scaffolds for potential cartilage repair applications, Int. J. Biol. Macromol. 114 (2018) 270–282.

[49] K. Theerakittayakorn, T. Bunprasert, Differentiation capacity of mouse L929 fibroblastic cell line compare with human dermal fibroblast, Int. J. Med. Heal. Sci. 5 (2011) 51–54.

[50] M. Weber, H. Steinle, S. Golombek, L. Hann, C. Schlensak, H.P. Wendel, M. Avci-Adali, Blood-contacting biomaterials: *in vitro* evaluation of the hemocompatibility, Front. Bioeng. Biotechnol. 6 (2018) 99.

[51] Q. Qian, K.A. Nath, Y. Wu, T.M. Daoud, S. Sethi, Hemolysis and acute kidney failure, Am.

J. Kidney Dis. 56 (2010) 780–784.

[52] D. Fischer, Y. Li, B. Ahlemeyer, J. Krieglstein, T. Kissel, In vitro cytotoxicity testing of polycations: influence of polymer structure on cell viability and hemolysis, Biomaterials. 24 (2003) 1121–1131.

[53] D. Chauhan, V. Nirbhaya, C.M. Srivastava, R. Chandra, S. Kumar, Nanostructured transition metal chalcogenide embedded on reduced graphene oxide based highly efficient biosensor for cardiovascular disease detection, Microchem. J. 155 (2020) 104697.

[54] W. Huang, A.K. Diallo, J.L. Dailey, K. Besar, H.E. Katz, Electrochemical processes and mechanistic aspects of field-effect sensors for biomolecules, J. Mater. Chem. C. 3 (2015) 6445–6470.

[55] Y. Chen, L.P. Mei, J.J. Feng, P.X. Yuan, X. Luo, A.J. Wang, Simple one-pot aqueous synthesis of 3D superstructured PtCoCuPd alloyed tripods with hierarchical branches for ultrasensitive immunoassay of cardiac troponin I, Biosens. Bioelectron. 145 (2019) 111638.

[56] S. Kumar, S. Kumar, S. Tiwari, S. Srivastava, M. Srivastava, B.K. Yadav, S. Kumar, T.T. Tran, A.K. Dewan, A. Mulchandani, Biofunctionalized nanostructured zirconia for biomedical application: a smart approach for oral cancer detection, Adv. Sci. 2 (2015) 1500048.

[57] N. Chaudhary, A.K. Yadav, J.G. Sharma, P.R. Solanki, Designing and characterization of a highly sensitive and selective biosensing platform for ciprofloxacin detection utilizing lanthanum oxide nanoparticles, J. Environ. Chem. Eng. 9 (2021) 106771.

[58] D. Verma, D. Chauhan, M. Das Mukherjee, K.R. Ranjan, A.K. Yadav, P.R. Solanki, Development of MWCNT decorated with green synthesized AgNps-based electrochemical sensor for highly sensitive detection of BPA, J. Appl. Electrochem. 51 (2021) 447–462.

[59] E. Spain, S. Carrara, K. Adamson, H. Ma, R. O'Kennedy, L. De Cola, R.J. Forster, Cardiac troponin I: ultrasensitive detection using faradaic electrochemical impedance, ACS Omega. 3 (2018) 17116–17124.

[60] S. Srivastava, V. Kumar, M.A. Ali, P.R. Solanki, A. Srivastava, G. Sumana, P.S. Saxena, A.G. Joshi, B.D. Malhotra, Electrophoretically deposited reduced graphene oxide platform for food toxin detection, Nanoscale. 5 (2013) 3043–3051.

[61] H. Bhardwaj, M.K. Pandey, G. Sumana, Electrochemical Aflatoxin B1 immunosensor based on the use of graphene quantum dots and gold nanoparticles, Microchim. Acta. 186

(2019) 1–12.

[62] V. Nirbhaya, D. Chauhan, R. Jain, R. Chandra, S. Kumar, Nanostructured graphitic carbon nitride based ultrasensing electrochemical biosensor for food toxin detection, Bioelectrochemistry. 139 (2021) 107738.

[63] J. Okuno, K. Maehashi, K. Kerman, Y. Takamura, K. Matsumoto, E. Tamiya, Label-free immunosensor for prostate-specific antigen based on single-walled carbon nanotube array-modified microelectrodes, Biosens. Bioelectron. 22 (2007) 2377–2381.

[64] Y. Wei, C. Gao, F.L. Meng, H.H. Li, L. Wang, J.H. Liu, X.J. Huang, SnO_2/reduced graphene oxide nanocomposite for the simultaneous electrochemical detection of cadmium (II), lead (II), copper (II), and mercury (II): an interesting favorable mutual interference, J. Phys. Chem. C. 116 (2012) 1034–1041.

[65] S. Kumar, J.G. Sharma, S. Maji, B.D. Malhotra, Nanostructured zirconia decorated reduced graphene oxide based efficient biosensing platform for non-invasive oral cancer detection, Biosens. Bioelectron. 78 (2016) 497–504.

[66] Y. Wan, Y. Su, X. Zhu, G. Liu, C. Fan, Development of electrochemical immunosensors towards point of care diagnostics, Biosens. Bioelectron. 47 (2013) 1–11.

[67] S. Zhang, F. Zheng, Z. Wu, G. Shen, R. Yu, Highly sensitive electrochemical detection of immunospecies based on combination of Fc label and PPD film/gold nanoparticle amplification, Biosens. Bioelectron. 24 (2008) 129–135.

[68] S. Kumar, S. Kumar, C.M. Pandey, B.D. Malhotra, Conducting paper based sensor for cancer biomarker detection, in: J. Phys. Conf. Ser., IOP Publishing, 2016: p. 12010.

[69] D. Chauhan, Y. Kumar, R. Chandra, S. Kumar, Nanostructured zirconia@ reduced graphene oxide based ultraefficient nanobiosensing platform for food toxin detection, Sensors & Diagnostics. 1 (2022) 550–557.

[70] M.A. Sadique, S. Yadav, P. Ranjan, R. Khan, F. Khan, A. Kumar, D. Biswas, Highly sensitive electrochemical immunosensor platforms for dual detection of SARS-CoV-2 antigen and antibody based on gold nanoparticle functionalized graphene oxide nanocomposites, ACS Appl. Bio Mater. 5 (2022) 2421–2430.

[71] P.K. Gupta, Z.H. Khan, P.R. Solanki, One-step electrodeposited porous ZnO thin film based immunosensor for detection of Vibrio cholerae toxin, J. Electrochem. Soc. 163 (2016) B309.

[72] S. Kumar, S. Kumar, S. Augustine, B.D. Malhotra, Protein functionalized nanostructured zirconia based electrochemical immunosensor for cardiac troponin I detection, J. Mater. Res. 32 (2017) 2966–2972.

[73] J. Bhardwaj, S. Devarakonda, S. Kumar, J. Jang, Development of a paper-based electrochemical immunosensor using an antibody-single walled carbon nanotubes bio-conjugate modified electrode for label-free detection of foodborne pathogens, Sensors Actuators B Chem. 253 (2017) 115–123.

[74] R. Singh, S. Kashyap, S. Kumar, S. Abraham, T.K. Gupta, A.M. Kayastha, B.D. Malhotra, P.S. Saxena, A. Srivastava, R.K. Singh, Excellent storage stability and sensitive detection of neurotoxin quinolinic acid, Biosens. Bioelectron. 90 (2017) 224–229.

[75] R. Singh, S. Hong, J. Jang, Label-free detection of influenza viruses using a reduced graphene oxide-based electrochemical immunosensor integrated with a microfluidic platform, Sci. Rep. 7 (2017) 42771.

[76] S. Kumar, S. Kumar, S. Tiwari, S. Augustine, S. Srivastava, B.K. Yadav, B.D. Malhotra, Highly sensitive protein functionalized nanostructured hafnium oxide based biosensing platform for non-invasive oral cancer detection, Sensors Actuators B Chem. 235 (2016) 1–10.

[77] Y. Chen, X.Y. Ge, S.Y. Cen, A.J. Wang, X. Luo, J.J. Feng, Ultrasensitive dual-signal ratiometric electrochemical aptasensor for neuron-specific enolase based on Au nanoparticles@ Pd nanoclusters-poly (bismarck brown Y) and dendritic AuPt nanoassemblies, Sensors Actuators B Chem. 311 (2020) 127931.

[78] E.B. Aydın, M. Aydın, M.K. Sezgintürk, A novel electrochemical immunosensor based on acetylene black/epoxy-substituted-polypyrrole polymer composite for the highly sensitive and selective detection of interleukin 6, Talanta. 222 (2021) 121596.

SUPPORTING INFORMATION

Figure S1

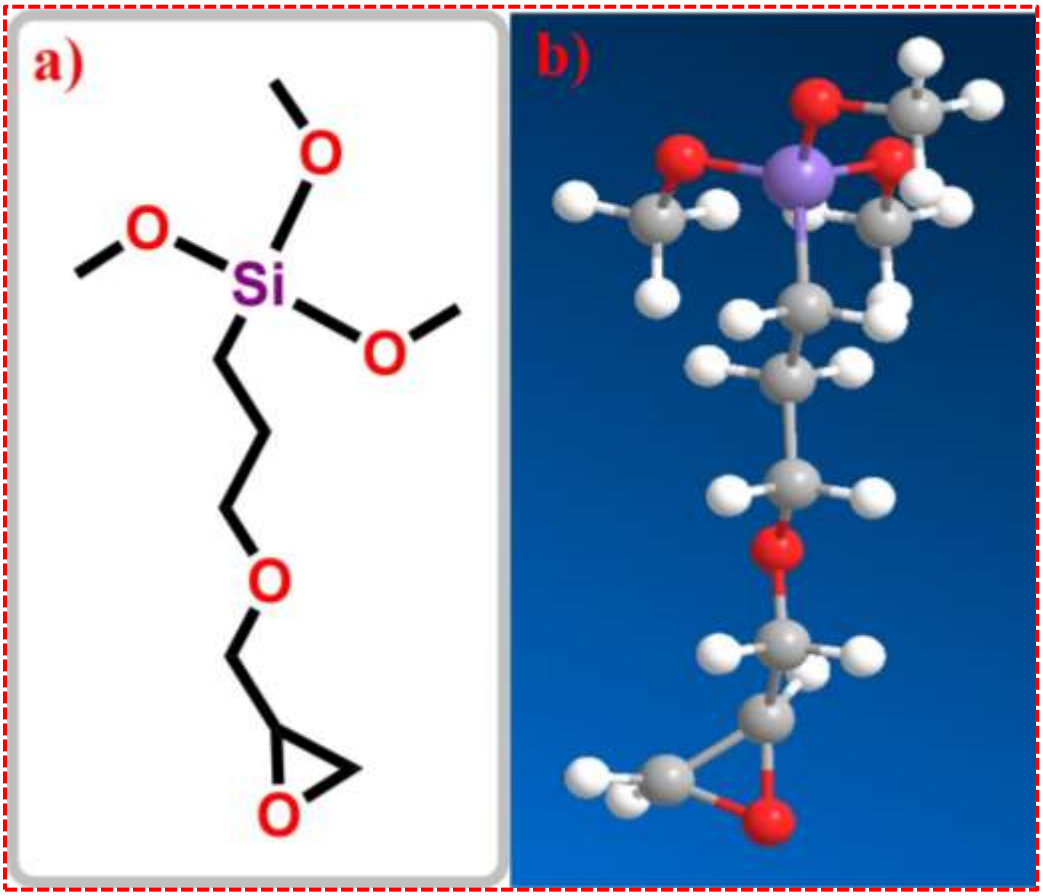

Figure S1. The 2D (A) and 3D (B) molecular structure of GPTMS.

Scheme S1

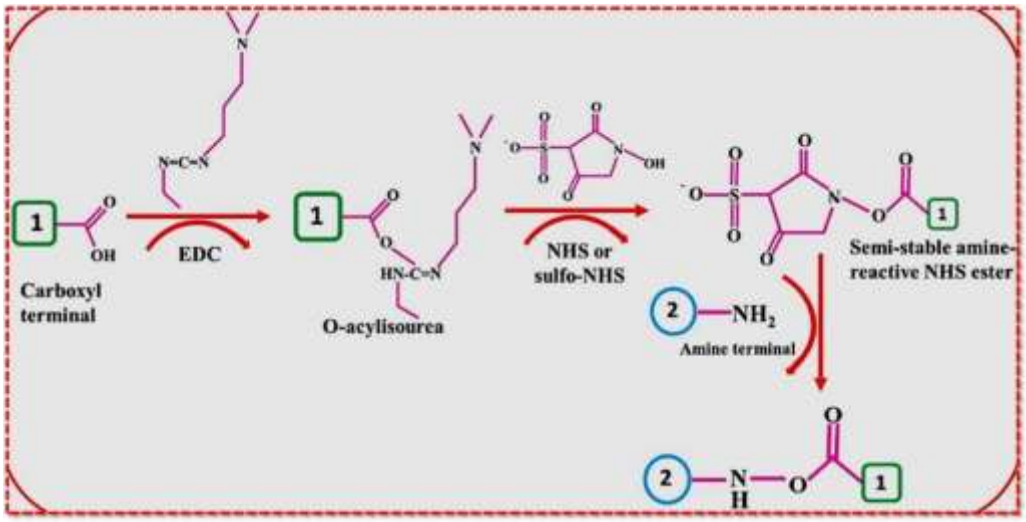

Scheme S1: Schematic chemical illustration of anti-SP17 antibodies immobilization on GPTMS@SAMs through EDC-NHS mechanism.

Figure S2

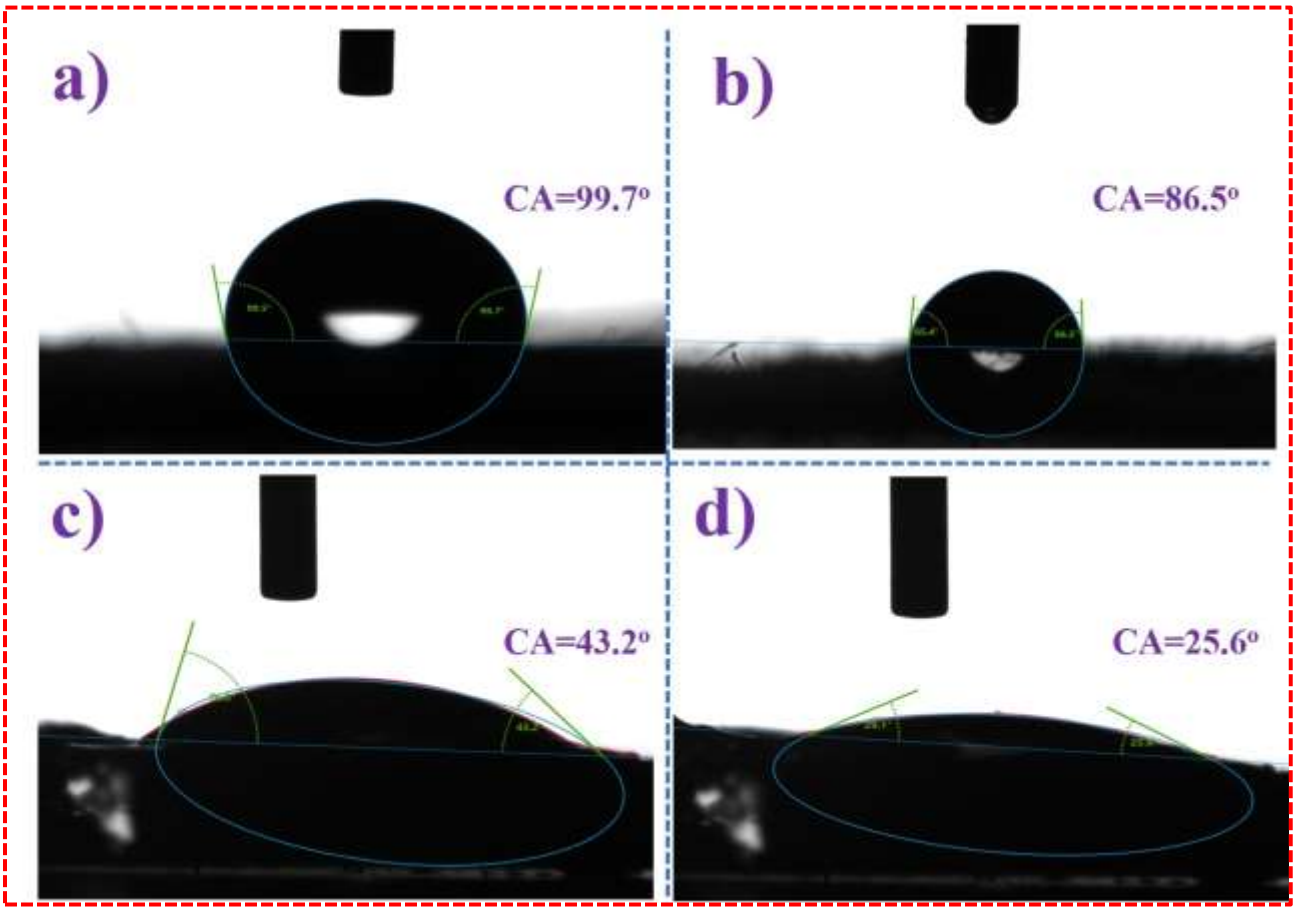

Figure S2. Water contact angle of ITO (a), GPTMS@SAMs/ITO (b), anti-SP17/GPTMS@SAMs/ITO (c) and BSA/anti-SP17/GPTMS@SAMs/ITO (d).

Figure S3

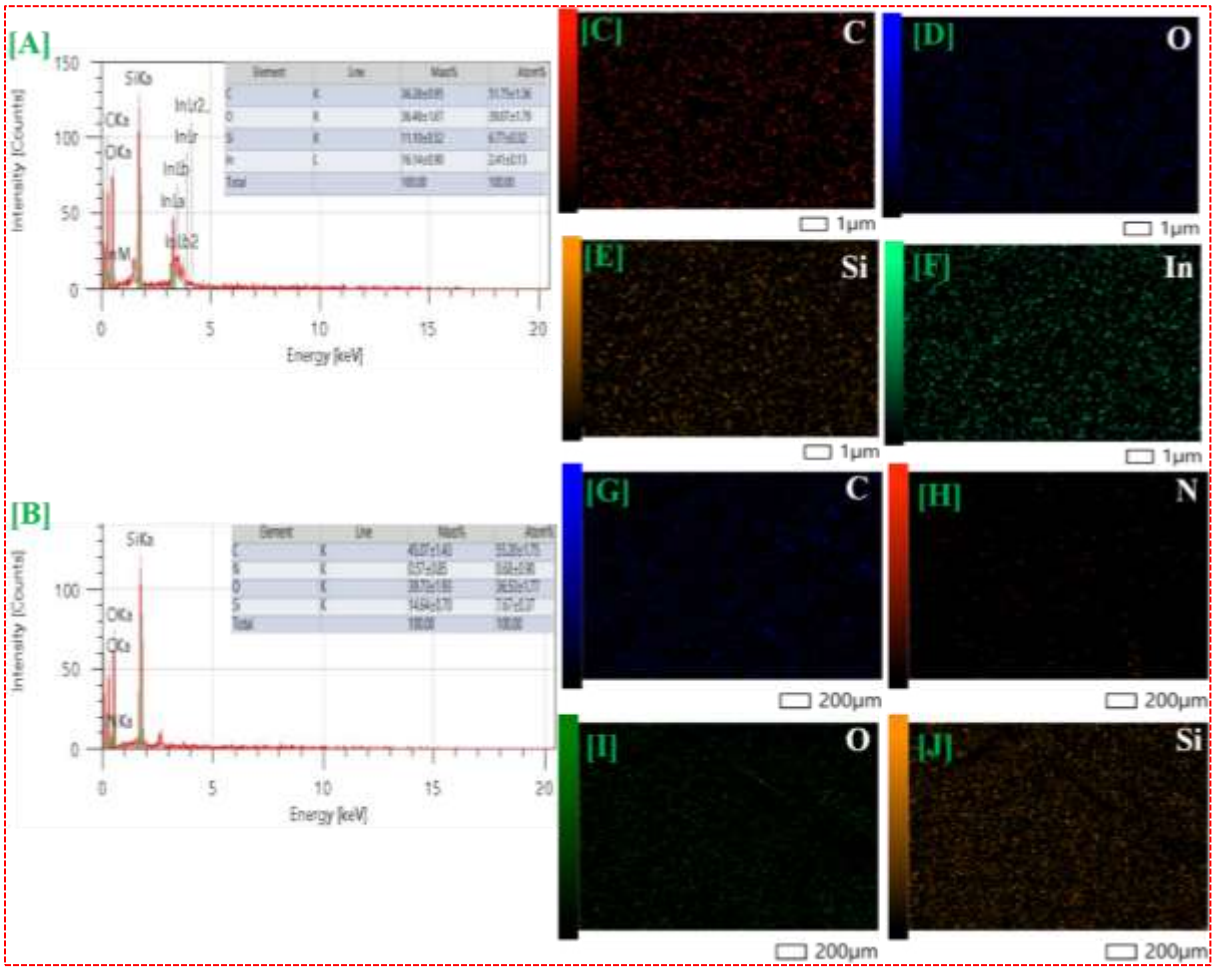

Figure S3. EDX spectrum and Elemental mapping of GPTMS@SAMs/ITO (A; C-F) and anti-SP17/GPTMS@SAMs/ITO electrodes (B; G-J). No external elements in the EDX spectra were observed, excluding the Indium background, signifying the pure quality of fabricated GPTMS@SAMs/ITO and anti-SP17/GPTMS@SAMs/ITO electrodes.

S1. ***Optimization of analytical variables***

To increase the efficiency of fabricated immunosensor, certain experimental conditions are tuned such as GPTMS (1% in toluene) volume, antibody concentration and incubation time, and BSA concentration. These parameters are necessary to fabricate an immunosensor that is sensitive, stable, repeatable, and reproducible.

Silane optimization is necessary as it provides the attachment sites for the biorecognition element. Therefore, firstly the effect of GPTMS concentration on the biosensor signal was studied, because this step affected the binding property of anti-SP17 antibody to ITO electrode surface. For this

examination, 6 different volumes of GPTMS (10-60 μL) were utilized. The highest signal was measured when 40 μL of GPTMS was utilized, then after current get saturated [Fig. S4(A)]. Thus, 40 μL GPTMS (11 % in toluene) volume was used to develop SAMs layer on ITO substrate.

Second optimization parameter was the anti-SP17 antibody concentration that utilized during the experiments. In this step, seven different concentrations (10 μg mL^{-1}, 20 μg mL^{-1}, 30 μg mL^{-1}, 40 μg mL^{-1}, 50 μg mL^{-1}, 60 μg mL^{-1} and 70 μg mL^{-1}) were utilized. Maximum signal was obtained when 50 μg mL^{-1} anti-SP17 antibody was utilized as bio-recognition molecule, as illustrated in [Fig. S4(B)]. Low concentration of anti-SP17 antibody immobilized ITO electrode could not determine SP17 antigen accurately. High concentration of anti-SP17 antibody may be formed higher steric barrier and the destructive effect of protein-protein interactions inhibiting the recognition of SP17 antigen .

Incubation time is another important parameter during the fabrication. Therefore, anti-SP17 antibody time were optimized. For anti-SP17 antibody incubation time optimization, max signal was obtained when the bioelectrode incubated at 6 h in anti-SP17 antibody solution and then got saturated. Less than 6 h as incubation time was not enough for anti-SP17 antibody immobilization, thus 6 h time is used as incubation time [Fig. S4(C)].

Further, Fig. S4(D) depicts peak current changes in the BSA/anti-SP17/GPTMS@SAMs/ITO immunoelectrode by varying the concentration of BSA from 0.1 to 4%. The rise in peak current was seen from 0.1 to 2%, after that it becomes stable. Thus, 2% BSA was chosen for fabricating the electrodes.

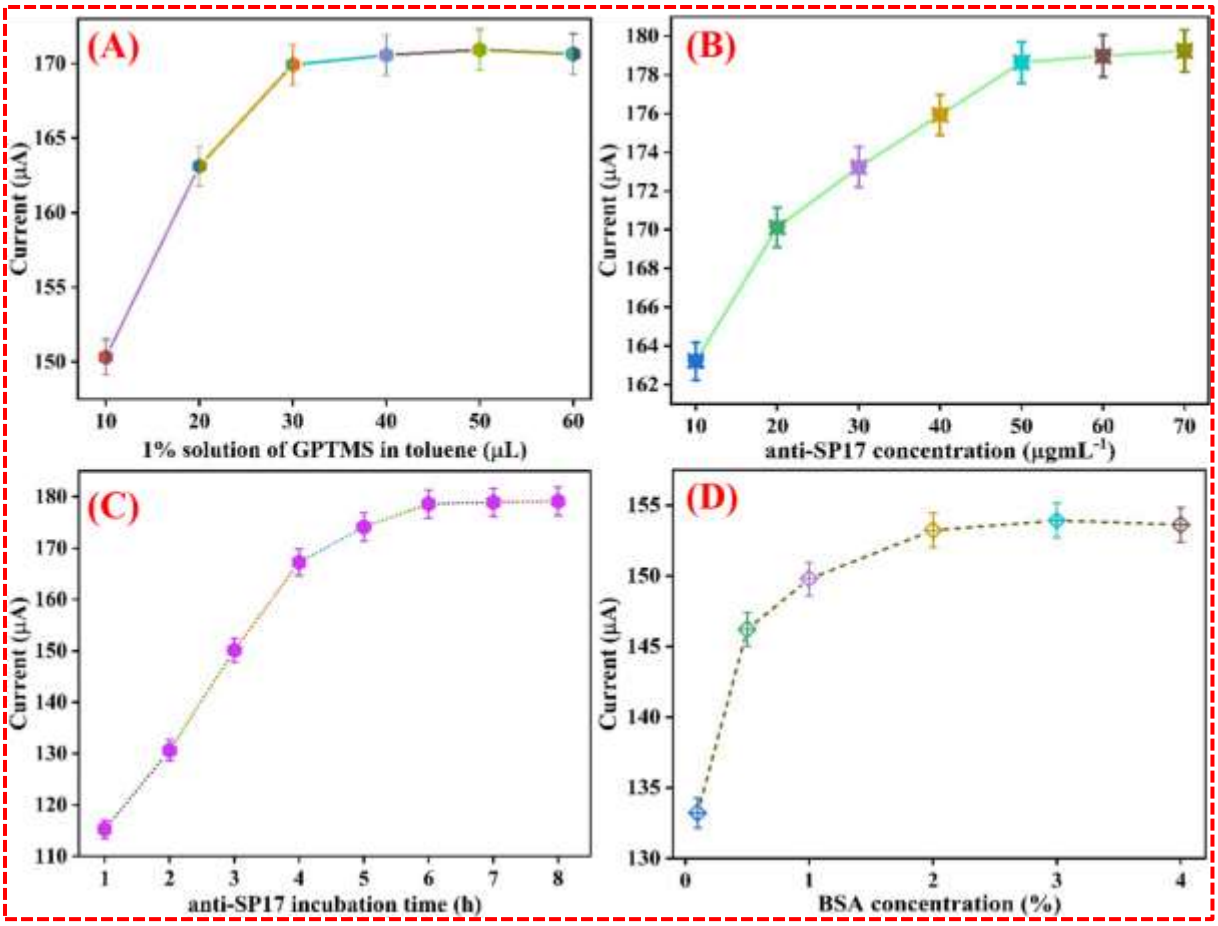

Figure S4. Optimization of various parameters of a biosensor. (A) effect of GPTMS volume on SAMs formation; (B) effect of different concentration of anti-SP17; (C) effect of incubation time of anti-SP17; (D) effect of different BSA concentration.

Table S1: Optimized values of different experimental factors.

GPTMS volume (1% in toluene)	10, 20, 30, 40, 50, and 60 μL	40 μL
anti-SP17 conc.	10, 20, 30, 40, 50, 60 and μgmL^{-1}	50 μgmL^{-1}
anti-SP17 incubation time	1, 2, 3, 4, 5, 6, 7, and 8 h	6 h
BSA concentration	01, 0.5, 1, 2, 3, 4 %	2 %

S2. Electrochemical Impedance spectroscopy (EIS) study

Electrochemical Impedance Spectroscopy (EIS) is a powerful electrochemical technique to detect biomolecules. One advantage of EIS over other methods is that it offers label-free and real-time detection by measuring small changes in the electrode-electrolyte interface impedance to detect and quantify probe-analyte interactions. EIS does not require any molecular modifications or labels, as is required in other systems, such as fluorescent-based or magnetic-based biosensors. Furthermore, it is possible to monitor the impedance changes that occur in real-time, i.e., as the surface binding occurs. EIS is an effective way to monitor the surface-modified electrode properties, and thus it allows the understanding of chemical transformation and processes formed on the electrode surface.

Moreover, EIS was a successful technique in investigating the bulk and interfacial electrochemical features of semi-conductive surfaces. Fig. 4(D) illustrates the Nyquist plot of the step-by-step modified electrodes and Fig. S5 show the Randle's equivalent circuit. As seen in Fig. 4(D), firstly, a low impedance response was observed on the ITO electrode after hydroxylation by using a mixed solution (1.98 kΩ; curve i). After GPTMS modification of the ITO electrode, an increase was seen in impedance response and charge transfer resistance that indicated the active electrochemical molecules transfer was prevented (3.82 kΩ; curve ii). Epoxysilane monolayer formed a barrier, and thus redox probe could not diffuse to the electrode surface. This observation was consistent with the results in the literature. Also, GPTMS SAMs led to a large Nyquist plot diameter than hydroxylated ITO electrodes. After anti-SP17 antibody immobilization on the electrode surface, a decrease in charge transfer resistance was seen (2.25 kΩ; curve iii), which indicated the chemical covalent bonding between epoxy groups of GPTMS and amino groups of anti-SP17 antibodies. This is due to the spatial alignment of the anti-SP17 molecule on the surface of the electrode that provides fast charge transfer among the unbound functional group (-NH_2) of anti-SP17 and redox species. Then, BSA was immobilized on the electrode surface to block the remaining epoxy ends; thus, the electron transfer resistance increased (6.52 kΩ; curve iv). This happens due to the insulating nature of BSA that inhibits the charge transfer process between the redox species and electrode surface.

The heterogeneous rate constant, i.e., Kct for the different fabricated electrodes, was estimated utilizing Eq. (S1).

$$\mathrm{Kct} = \frac{RT}{n^2F^2\mathrm{ARct[S]}} \quad \text{.....Eq.(S1)}$$

Where '[S]' is the concentration of redox probe (mol cm^{-3}), 'F' depicts the Faraday constant; 'A' shows the surface area of the electrode (cm^2), 'n' represents the number of electrons transferred/molecule of the $[Fe(CN)_6]^{3-/4-}$, 'T' is the absolute temperature, and 'R' is gas constant. The K_{ct} value of the ITO electrode was found as $4.42 \times 10^{-7,}$ while in the case of GPTMS@SAMs/ITO, the value of K_{ct} decreases to 1.24×10^{-7}, exhibiting the slower electron transfer between the GPTMS@SAMs/ITO electrode and $[Fe(CN)_6]^{3-/4-}$. After attaching anti-SP17 antibodies, the K_{ct} value increases to $2.62 \times 10^{-7,}$ showing the fast electron exchange between immunoelectrode and redox species. However, after the BSA immobilization on anti-SP17/GPTMS@SAMs/ITO immunoelectrode, the value of K_{ct} decreases to 1.70×10^{-7} due to its insulating nature, which resists the transfer of electrons.

The Time constant (τ) for each electrode has been calculated using the given equation below

$$Rct.Cdl = 1/2\pi\ fmax = \tau \quad \text{Eq. (S2)}$$

After the formation of GPTMS SAMs on the ITO substrate (2.356×10^{-3} s), an abrupt increase in the time constant value was found compared to the ITO glass substrate 5.744×10^{-3} s. It reveals the slow diffusion of ferro-ferri ions at the electrolyte and GPTMS@SAMs/ITO electrode interface. The immobilization of anti-SP17 onto the GPTMS@SAMs/ITO resulted in a decrease of τ value 4.009×10^{-3} s due to the rapid diffusion of Ferro-ferri ions. After the BSA immobilization, the value of τ again increases by 4.637×10^{-3} s) due to the insulating behavior of BSA. EIS characteristics, including Kct and τ, s of different electrodes, were given in Table S2.

Table S2. EIS features of various electrodes

Electrode	**Charge transfer** Resistance (R_{ct})	**Heterogeneous electron** transfer rate constant [K_{ct} (cms^{-1})]	Time constant (τ) s
ITO	1980 Ω	1.24×10^{-7}	2.356×10^{-3}
GPTMS@SAMs/ITO	3820 Ω	1.69×10^{-7}	5.744×10^{-3}
anti-SP17/GPTMS@SAMs/ITO	2250 Ω	2.46×10^{-7}	
BSA/anti-SP17/GPTMS@SAMs/ITO	6520 Ω	4.42×10^{-7}	4.009×10^{-3}

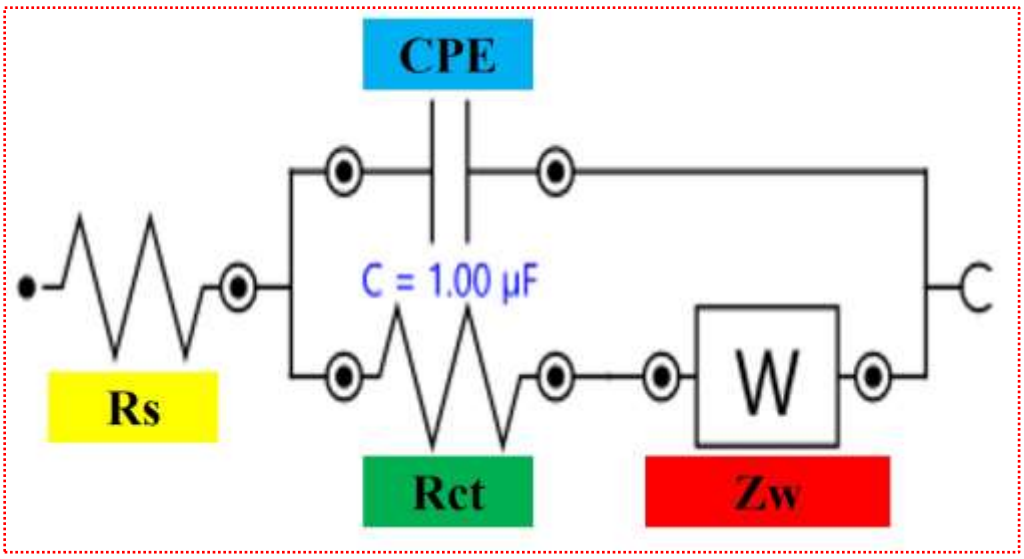

Figure S5: Randle's equivalent circuit.

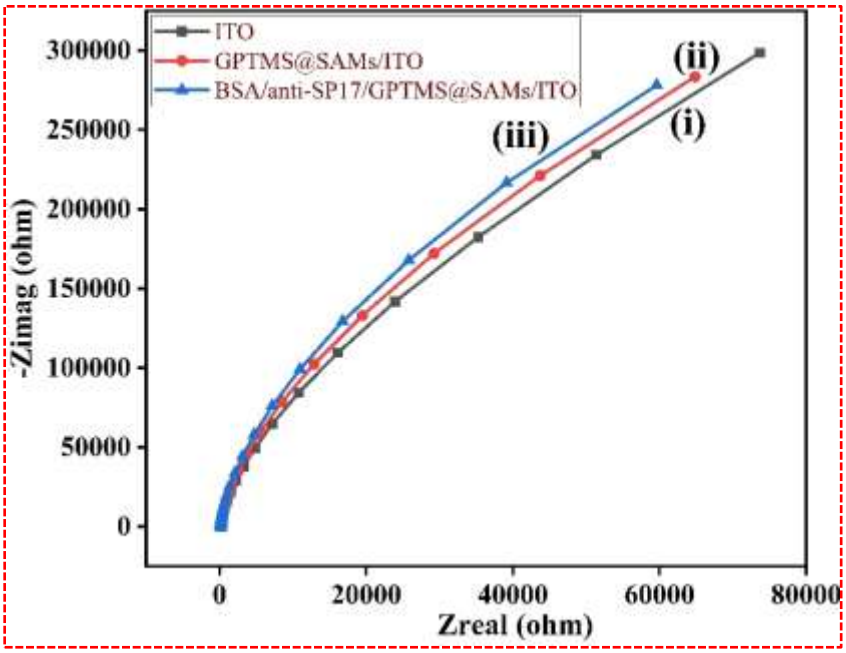

Figure S6: Frequency response analysis (FRA) of (i) ITO, (ii) GPTMS@SAMs/ITO, (c) BSA/anti-Sp17/GPTMS@SAMs/ITO immunoelectrode in PBS only (pH 7.0) at a zero potential in the frequency range of 100 kHz–10 Hz.

Table S3: Parameters observed during EIS studies in PBS

Electrode	Rs (Ω)	Rct (TΩ)	C(μF)	Zw (Mho)
ITO	170	-1.10	4.36	1.10
GPTMS@SAMs/ITO	158	-1.10	4.72	1.10
BSA/anti-SP17/ GPTMS@SAMs/ITO	144	-1.10	4.90	1.10

S3. Scan rate studies

To examine the effect of scan rate, the electrochemical CV response was studied on the GPTMS@SAMs/ITO and BSA/anti-SP17/GPTMS@SAMs/ITO electrodes at the interface of the electrode surface and electrolyte as a function of scan rate in the range 10–100 mVs^{-1} and the obtained results are shown in Fig. 4(E) and 4(F) respectively. In case of both electrode the magnitudes of anodic (Ipa) and cathodic (Ipc) peak currents increased linearly with increasing scan rate indicating that the electrochemical reaction is in a diffusion control process. The Fig. 4(E) and 4(F) (upper inset) shows the variation of anodic (Ipa) and cathodic (Ipc) peak current vs square root of scan rate. In both electrodes the magnitude of current linearly increased with increase in scan rates and follow Eqs. (S3)–(S6):

$Ipa_{(GPTMS@SAMs/ITO)}$=[28.73μA(s/mV)×(scan rate [mV/s])$^{1/2}$]–13.451μA, R^2 = 0.999…Eq.(S3)

$Ipc_{(GPTMS@SAMs/ITO)}$=-[22.71μA(s/mV)×(scan rate [mV/s])$^{1/2}$]–20.66μA, R^2= 0.997…..Eq.(S4)

$Ipa_{(BSA/anti-SP17/GPTMS@SAMs/ITO)}$=[21.39μA(s/mV)×(scan rate [mV/s])$^{1/2}$]-1.73μA, R^2=0.998 Eq.(S5)

$Ipc_{(BSA/anti-SP17/GPTMS@SAMs/ITO)}$=-[13.42μA(s/mV)×(scan rate [mV/s])$^{1/2}$]-47.07μA, R^2= 0.984 Eq.(S6)

Moreover, the peak-to-peak separation was shifted with increasing scan rate as shown in Fig. 4(E) and 4(F) (lower inset), which concluded that the procedure is electrochemically quasi-reversibl. The difference in the peak potentials of cathodic (Epc) and anodic (Epa) (ΔEp = Epa- Epc) as a function of the square root of scan rate for GPTMS@SAMs/ITO and BSA/anti-SP17/GPTMS@SAMs/ITO electrodes demonstrated a linear relationship given by the Eq. (S7) and (S8). It suggested a facile transfer of electrons from medium to the electrode.

$\Delta Ep_{(GPTMS@SAMs/ITO)}$=[0.030V(s/mV)×(scan rate [mV/s])$^{1/2}$]+0.510V, R^2= 0.967……..Eq.(S7)

$\Delta Ep_{(BSA/anti\text{-}SP17/GPTMS@SAMs/ITO)}$=[0.013V(s/mV)×(scan rate [mV/s])$^{1/2}$]+1.016V, R^2 = 0.987 Eq.(S8)

The diffusion coefficient (D) was estimated using the Randles-Sevcik equation [S9], at the bioelectrode surface and electrolyte interface having redox species $[Fe(CN)_6]^{3-/4}$:

$$Ip = (2.69\times10^5)\, C\, n^{3/2}\, D^{1/2}\, \upsilon^{1/2}\, A \text{……..……. Eq.(S9)}$$

Where I_p (I_{pa} or I_{pc}) symbolizes the peak current of electrodes, 'n', number of electrons involved in the redox event (= 1 here), A is the active surface area of bioelectrode (0.25 cm^2), D is the diffusion coefficient (cm^2s^{-1}), C is the concentration of electrolyte species (0.2 mM), and υ is scan rate (50 mVs^{-1}). The lower value of D demonstrated for BSA/anti-SP17/GPTMS@SAMs/ITO immunoelectrode (0.0414×10^{-18} cm^2s^{-1}) indicates a lower rate of transfer of electron kinetics at the interface of electrolyte/electrode in comparison to GPTMS@SAMs/ITO electrode (0.0638×10^{-18} cm^2s^{-1}) resulting in superior analytical efficiency of this biosensor [4]. Therefore, diffusion coefficient depends on the surface area of the working electrode and on the concentration of electro-active species.

To calculate the value of the efficient and effective electroactive surface area (A_e) of the unmodified electrode GPTMS@SAMs/ITO electrode and BSA/anti-SP17/GPTMS@SAMs/ITO immunoelectrode, the calculated value of D has been put in the following equation [3]:

$$A_e = \frac{S}{(2.69\times10^5)n^3\, CD^{1/2}} \text{…… Eq.(S10)}$$

Where *S*, the slope of the linear curve obtained from the plot between Ipa versus square root of scan rate ($v^{1/2}$) [in $(mV/s)^{1/2}$]. The value of BSA/anti-SP17/GPTMS@SAMs/ITO immunoelectrode's electroactive area (A_e) is 23387.27×10^4 which revealed that these are more suitable having more reaction sites/unit volume due to immobilization of biomolecules (i.e., BSA and antibody) as compared to GPTMS@SAMs/ITO electrode (13350.37×10^4 mm^2).

Furthermore, the surface concentration of the absorbed electroactive ionic species (I^* in mol cm^2) for the corresponding electrodes has been calculated using Brown-Anson equation, as stated below;

$$I_p = \frac{n^2 F^2 \gamma^* A \upsilon}{4 R T} \text{.....Eq.(S11)}$$

Where I_p (I_{pa} or I_{pc}) denotes the peak current, A is the electrode surface area, γ is the surface concentration of the absorbed electro-active species, υ is the scan rate (Vs^{-1}), F- the Faraday constant (96485 C mol^{-1}), T- room temperature (298 K), and R- gas constant (8.314 mol^{-1} K^{-1}). The approximate value of surface concentration (γ^*) for BSA/anti-SP17/GPTMS@SAMs/ITO immunoelectrode (1.17×10^{-11} mol cm^2) is higher as compared to GPTMS@SAMs/ITO electrode (1.45×10^{-11} mol cm^2), which reveals an enhancement in the electrocatalytic behavior at its surface due to the presence of biomolecules and BSA which can be used for the biosensing applications.

The electron transfer reversibility kinetics depends on the scan rate as well as on heterogeneous electron transfer rate constant (K_s). The values of K_s for GPTMS@SAMs/ITO electrode and BSA/anti-SP17/GPTMS@SAMs/ITO immunoelectrode are 1529.74 s^{-1} and 2214.45 s^{-1}, respectively, estimated by Laviron Equation. The bioelectrode had higher K_s value indicating that the electron exchange is fast between the surface of the electrode and electrolyte redox species.

$$K_s = \frac{mn\,Fv}{RT} \text{.....Eq.(S12)}$$

where, m- the peak-to-peak separation of potentials (V).

The calculated values of various electrochemical parameters; cathodic peak current (Ipc), anodic peak current (Ipa), charge transfer rate constant (K_s), diffusion coefficient (D), average surface concentration (γ^*), electroactive surface area (A_e), of ionic species of the respective electrodes were given in Table S3. The higher values of the interface kinetic parameters of the BSA/anti-SP17/GPTMS@SAMs/ITO immunoelecrode as compare to GPTMS@SAMs/ITO electrode suggests that biomolecules such as Ab and BSA are significantly contributed to the enhancement of electron transfer at bioelectrode and electrolyte interface.

Table S3. Projected values of electrochemical factors for electrodes

Electrode	D ($cm^2 s^{-1}$)	A_e (mm^2)	I^*(mol cm^2)	K_s (s^{-1})	I_{pa} (A)	I_{pc} (A)
ITO	0.0798×10^{-18}	-	1.63×10^{-11}	896.88	$1.90E^{-4}$	$1.83E^{-4}$
GPTMS@SAMs/ITO	0.0638×10^{-18}	13350.37×10^{4}	1.45×10^{-11}	1529.74	$1.70E^{-4}$	$1.67E^{-4}$
anti-SP17/GPTMS@SAMs/ITO	0.0700×10^{-18}	-	1.52×10^{-11}	1317.18	1.78^{-4}	$2.10E^{-4}$
BSA/anti-SP17/GPTMS@SAMs/ITO	0.0414×10^{-18}	23387.27×10^{4}	1.17×10^{-11}	2214.45	$1.37E^{-4}$	$1.31E^{-4}$

“MSIPFSNTHYRIPQGFGNLLEGLTREILREQPDNIPAFAAAYFE
SLLEKREKTNFDPAEWGSKVEDRFYNNHAFEEQEPPEKSDPK
QEESQISGKEEETSVTILDSSEEDKEKEEVAAVKIQAAFRGHIA
REEAKKMKTNSLQNEEKEENK”.

Figure S7: Amino acid sequence of SP17 antigen

S4. Calculation of number of molecules in SP17 at LOD of 47.57 $pgmL^{-1}$:

Molecular weight of SP17 = 24.5 kDa or 24.5×10^3 g mol^{-1}

Concentration (strength) of SP17 solution at LOD = 47.57 $pgmL^{-1}$ or 4.8×10^{-8} g L^{-1}

Thus, molarity of solution = strength/ molecular weight

$= 4.8\times10^{-8}$ g L^{-1}/ $36 \times 24.5 \times 10^3$ g mol^{-1}

$= 1.95\times 10^{-12}$ mol L^{-1}

Number of molecules of SP17 in this concentration

= Molarity × Avogadro number

$= 1.95\times 10^{-12}$ mol $L^{-1}\times 6.022 \times 10^{23}$ molecules mol^{-1}

$= 1.1 \times 10^{12}$ molecules L^{-1}

So, number of molecules in 1 L or 10^6 μL of solution = 1.1×10^{12} molecules

Therefore, Number of molecules in 20 µL of solution

$$= 1.1 \times 10^{12} \text{ molecules} \times 20\ \mu L / 10^{6}\ \mu L$$

$$= 22 \times 10^{7} \text{ molecules}/20\ \mu L$$

Hence, 20 µL of 47.57 $pgmL^{-1}$ solution contains ~ 22×10^{7} molecules of SP17

Amit Kr Yadav
31/8/2023